12-1-2014

Novel Deployment of Elpasolites as a Dual Neutron / Gamma-ray Directional Detector

Amber Lynn Guckes
University of Nevada, Las Vegas, shield39@unlv.nevada.edu

NOVEL DEPLOYMENT OF ELPASOLITES AS A DUAL NEUTRON / GAMMA- RAY DIRECTIONAL DETECTOR

By

Amber Guckes

Bachelor of Science in Mechanical Engineering

University of Nevada, Las Vegas

2013

A thesis submitted in partial fulfillment

of the requirements for the

Master of Science - Materials and Nuclear Engineering

Department of Mechanical Engineering

Howard R. Hughes College of Engineering

The Graduate College

University of Nevada, Las Vegas

December 2014

This research was supported by National Security Technologies, LLC, under Contract No. DE AC52-06NA25946 with the U.S. Department of Energy. The United States Government retains and the publisher, by accepting the article for publication, acknowledges that the United States Government retains a non-exclusive, paid-up, irrevocable, world-wide license to publish or reproduce the published form of this manuscript, or allow others to do so, for United States Government purposes. DOE/NV/25946--2256.

UNLV | GRADUATE COLLEGE

We recommend the thesis prepared under our supervision by

Amber Guckes

entitled

Novel Deployment of Elpasolites as a Dual Neutron / Gamma-ray Directional Detector

is approved in partial fulfillment of the requirements for the degree of

Master of Science - Materials and Nuclear Engineering

Department of Mechanical Engineering

Alexander Barzilov, Ph.D., Committee Chair

William Culbreth, Ph.D., Committee Member

Denis Beller, Ph.D., Committee Member

Ke-Xun Sun, Ph.D., Graduate College Representative

Kathryn Hausbeck Korgan, Ph.D., Interim Dean of the Graduate College

December 2014

ABSTRACT

NOVEL DEPLOYMENT OF ELPASOLITES AS A DUAL NEUTRON / GAMMA-RAY DIRECTIONAL DETECTOR

by

Amber Guckes

Dr. Alexander Barzilov, Examination Committee Chair

Associate Professor of Mechanical Engineering

University of Nevada, Las Vegas

At a time when upholding national security has never been more important, there exists a need for the advancement of radiation detection technologies. Neutron and photon detectors are essential to fulfilling mission areas including detection and localization of missing, stolen or smuggled radiological or nuclear materials, quantification of the effects of a radiological or nuclear event, and supporting nonproliferation efforts. The aim of this study was to evaluate a new radiation detector based on the scintillation elpasolite compound Cs_2LiYCl_6:Ce (CLYC) for simultaneous measurements of neutron and photon flux and the localization of radiation sources. Previous studies performed on the CLYC scintillator indicate its potential for thermal neutron and gamma-ray measurements. This study is dedicated to the novel application of the CLYC as a dual neutron / photon detector and as part of a directional detection system.

Both computational modeling and an experimental study were carried out within this research project. As part of the computational study, the response of a CLYC scintillator detector to gamma rays induced by thermal neutron interaction with Cl and ^{7}Li nuclei was investigated using the MCNP6 code. In addition, arrays of three and four CLYC detectors were modeled in order to evaluate the directional detection of both a thermal neutron source and a gamma-ray source. It was shown that little or no quality of source direction determination would be lost when three detectors were used in the array compared to four detectors.

In the experimental study, the photon spectroscopy capabilities of the CLYC detectors were evaluated. A gamma-ray energy resolution of 4.9% was measured for the 662-keV peak of ^{137}Cs and 3.6% for the 1.33-MeV peak of ^{60}Co. Using a thermal neutron source, the pulse shape discrimination analysis was successfully performed for the CLYC detector signal waveforms. Thermal neutrons and gamma rays were separated with an exceptional figure of merit (FOM) of 2.3. An array of three CLYC detectors was assembled for the purpose of directional neutron / gamma-ray detection. The intrinsic peak efficiency of CLYC detectors was evaluated. The three-CLYC detector array was deployed for directional measurements with a single gamma-ray ^{137}Cs source, two gamma-ray sources of ^{137}Cs and ^{60}Co isotopes and a thermal neutron source designed using a ^{239}PuBe neutron source supplied with a polyethylene moderator. Measurements were carried out using sources located in the longitude and latitude planes over the angles from 0° to 360°. The measured data were processed through a maximum likelihood estimation algorithm providing a possible direction for which the radioactive source in each case was positioned. The estimated directions were close if not exact matches for

the actual directions to the radioactive source. The largest discrepancy in direction produced by the algorithm was approximately 11%. However, it was hypothesized that this percent error can be decreased by homogenizing the directional detection system to consist of scintillators of the same size and quality, identical photomultiplier tubes and identical aluminum housings. The feasibility of this hypothesis to decrease the percent error was confirmed by the zero percent error achieved in the directional measurements produced in the computational study utilizing a homogenous directional detection system.

The results of computational and experimental studies completed within this research project provide means to propose the array of three CLYC scintillators as an efficient dual neutron / gamma-ray directional detector.

ACKNOWLEDGEMENTS

Words cannot describe how blessed I am to have so many incredibly talented and caring people to which I owe my success in completing this thesis. This journey has been one of the most rewarding experiences of my life and I am beyond thankful that I was able to share it with you all.

First, I would like to thank my thesis committee members: Dr. Barzilov, Dr. Beller, Dr. Culbreth and Dr. Sun. Thank you for signing off on countless forms, reading hundreds of pages, guiding me down the right path and providing me with a lifetime of learning. A special thank you goes to Dr. Barzilov and Dr. Beller.

Dr. Barzilov, thank you for taking so much time to make sure I continued to learn and progress as a nuclear engineer. I have gained so much knowledge and experience from performing the research for my thesis, but also by conducting other research, writing publications and attending conferences to which you encouraged and guided me through. I believe I am ready and able to enter the workforce thanks to you.

Dr. Beller, I owe much of my success to you believing in me. Thank you for taking me in as a research assistant, providing me with my first opportunity to perform nuclear-related work and helping me achieve my professional goals. You have been a great mentor to me and I will always look up to you.

Thank you to Dr. Guss and the NSTec Remote Sensing Laboratory for allowing me to take part in such interesting and cutting edge research. I hope that one day we may work together again.

Thank you to my peers at UNLV. I am a fierce competitor, so thank you for pushing me to be my best through my undergraduate and graduate career. I am honored

to have learned with some of the best and brightest students in the world. A special thank you goes to Jessica Hartman and Norman Richardson for answering my endless questions and motivating me to be the best student I could be.

No one would be reading this thesis if it were not for my family. To my family I owe everything. Thank you to my mom who has stood by my side no matter what. Mom, you have loved me and supported me through so many up's and down's. I cannot put into words how much I appreciate everything you have done for me. Thank you to my dad, who is the reason why I am a nuclear engineer. Dad, you have always encouraged me to reach for the stars and never give up. Thank you for listening to me about my research and sharing the same passion about nuclear energy which I do. Your continuous love and guidance have made me the best nuclear engineer I can be today. To my brother Sean, thank you for believing in me and for your continued encouragement. Although we may be miles away from each other now, you continue to believe in me and listen to me when I need it most. Finally, to my husband, thank you for putting up with me through this entire last year. From never being home to being home and always glued to my laptop, books and papers to finish this thesis, I thank you for your understanding, motivation and for following me as I pursue so many crazy ideas. I couldn't have picked a better partner to accompany me on this journey. I love you all and I cannot wait to share the rest of my adventures with you.

DEDICATION

To my family.

Forever, for always & no matter what.

TABLE OF CONTENTS

LIST OF TABLES

LIST OF FIGURES

CHAPTER 1

INTRODUCTION

1.1 Background

During the early 1900s, the rate at which nuclear physics advanced was truly outstanding. Within a few short decades the discovery of the neutron, nuclear fission and nuclear chain reaction took place. These discoveries provoked the design and development of the atomic bomb, thermonuclear bomb and later, nuclear propulsion, nuclear medicine and nuclear power reactors. Scientists such as Ernest Rutherford, Niels Bohr, Marie Curie, Lise Meitner, Edward Teller, Leo Szilard, Enrico Fermi and J. Robert Oppenheimer offered vast contributions to these advancements in nuclear physics. Their efforts continue to resonate in nuclear research today.

However, these accomplishments may not have evolved as quickly as they did without a means to observe the existence of nuclear particles and the behaviors associated with each particle. So with these advancements came the progression of radiation detection technologies. One of the first forms of detecting ionizing radiation was by the light scintillations induced in a zinc sulfide, but was shortly shadowed by the development of other detectors including the electroscope, the cloud chamber and the Geiger-Mueller counter. Scintillation detection later came back to prominence along with the creation of proportional gas counters in the 1940s. These radiation detectors have continued to grow and have become essential to radiation detection applications today.

The need for reliable radiation detection technologies in the United States has increased with the heightened importance of national security, nuclear nonproliferation and safeguards efforts. Specific radiation detection applications include border

protection, detection of illicit materials in transportation, safeguards, treaty verification, remote sensing, homeland security, emergency response and monitoring of nuclear facilities to name a few.

A continuous effort to improve radiation detection technologies to meet the growing needs of the field is afforded by many scientists and engineers. Groups contributing to the advancement of radiation detection technologies include the U.S. Department of Homeland Security, U.S. Department of Defense, U.S. Department of Energy, national laboratories, government contractors, private industry and universities. The increased performance and capabilities of radiation detectors can be afforded to these groups. It is the purpose of this thesis to contribute to this effort by providing an evaluation of a new and emerging radiation detector technology.

1.2 Project Motivation

Nuclear nonproliferation and safeguards are areas of increased importance in the world today. Preventing the spread of special nuclear materials and radiological materials is an essential part to maintaining U.S. national security and global security. Groups such as the U.S. Department of Defense, Department of Homeland Security, Department of Energy, Nuclear Regulatory Commission, International Atomic Energy Agency and nuclear disaster first responders require radiation detection systems capable of detecting radioactive / nuclear material at very low concentrations and sometimes from a substantial distance. The ideal detector for such applications should have an appropriate energy resolution, high detection efficiency, compact size, be easily portable and cost efficient.

Currently, there exists no single detector that is commercially produced or widely used for the purposes of dual neutron / gamma-ray directional detection. Several dual neutron / gamma-ray detectors, directional detectors and dual neutron / gamma-ray directional detectors have been developed but possess limitations keeping each from being commercially produced and used widely in the field.

Thallium activated sodium iodide (NaI(Tl)) scintillators coupled with ^{3}He gas proportional counters are commonly used for the dual detection of gamma rays and neutrons, respectively. It is desired to simplify and improve this detection technology due to several key factors. The first factor is that the price of ^{3}He gas proportional counters is on the rise due to a lack of ^{3}He gas supply [1]. It is also desired to employ a scintillator with improved characteristics compared to NaI(Tl) and capable of simultaneous detection of neutrons and photons.

A project between National Security Technologies, LLC (NSTec), Remote Sensing Laboratory at Nellis Air Force Base in Las Vegas, NV, and the University of Nevada, Las Vegas has been formed to evaluate feasibility of a novel scintillating material deployed as a dual neutron / gamma-ray directional detector. The driving motives behind this project include developing an improved dual neutron / gamma-ray directional measurement technique to contribute to the effort in advancing radiation detection technologies to meet the rising needs of the nuclear enterprise. This thesis provides an in-depth review of the experiments and computational studies, discussion and results of this evaluation performed by the author.

1.3 Project Objectives

In the research described herein, the CLYC scintillator is evaluated as a high-performance directional neutron / gamma-ray detector. It is the purpose of this research, through experiments and computational modeling, to contribute to the understanding and applicability of the CLYC scintillator. The following subsections outline the steps used to perform this research project.

1.3.1 Neutron and Photon Measurements

Gamma-ray spectroscopy of the radiation emissions of isotopes cesium-137 (^{137}Cs) and cobalt-60 (^{60}Co) was utilized to evaluate the feasibility of the direct digital waveform analysis of the CLYC detector signals and to determine its gamma-ray energy resolution. Dual neutron / gamma-ray measurements using a sealed plutonium-beryllium (^{239}PuBe) source were carried out to evaluate the characteristics of the neutron and gamma-ray signals. The pulse shape discrimination (PSD) analysis of the detector signals was performed using a digitizer and multichannel analyzer (MCA). The data collected during this measurement via the four-channel digitizer and MCA qMorpho was used to evaluate the data acquisition system and to determine its optimal parameters.

1.3.2 Directional Measurements using the Detector Array

An array consisting of three CLYC detectors was studied for the directional detection of neutron and photon fluxes. An array of detectors allows the user to determine the position of the radiation source being detected. A maximum likelihood estimation algorithm (MLEA) was developed to determine the most probable location of the radiation source using the detector responses. The directional detection performance of

the array was evaluated in experiments using various radiation sources. Computational modeling was also performed studying CLYC detector responses to supplement the experimental results.

1.4 Radiation Detection Fundamentals

1.4.1 The Atom

All matter consists of atoms and all atoms consist of subatomic particles. Protons, neutrons and electrons are of particular interest in nuclear engineering. Each of these subatomic particles possesses characteristics that make it unique as shown in Table 1. In addition, photons that are emitted in nuclear and atomic transitions are important in radiation measurements.

The nuclei of atoms with various numbers of protons and neutrons are called nuclides. The atomic number describes the number of protons in a given nuclide. The atomic mass of a nuclide defines the number of protons plus the number of neutrons. Every nuclide has a different atomic number and atomic mass. Moreover, each type of nuclide possesses several isotopes. Isotopes share the same atomic number, but a different atomic mass and thus a different number of neutrons. There are stable and unstable isotopes. Stable isotopes do not transform into a different nuclide through decay processes; unstable isotopes do. Radioactive isotopes are unstable; they decay from one daughter nuclide to the next until a stable nuclide is formed.

Radioactive isotopes can transform by several decay mechanisms including alpha decay, beta decay, spontaneous fission, electron capture, isomeric transition, proton emission, neutron emission or heavy ion emission. The mode of radioactive decay

determines the daughter nuclides to which the original nuclide decays to. Some of the most common isotopes utilized in nuclear engineering are presented in Table 2.

Table 1 – Subatomic particles [2]

Subatomic Particle	Rest Mass (kg)	Charge (C)
Proton	1.672620×10^{-27}	$+1.602192\times 10^{-19}$
Neutron	1.674929×10^{-27}	Neutral
Electron	9.109390×10^{-31}	-1.602192×10^{-19}

Table 2 – Important isotopes in nuclear engineering [2]

Isotope	Atomic Number	Atomic Mass	Half-life (years)	Fissile / Fissionable
^{233}**U**	92	233.0396	1.592×10^{5}	Fissile
^{235}**U**	92	235.0439	7.038×10^{8}	Fissile
^{238}**U**	92	238.0508	4.68×10^{9}	Fissionable
^{239}**Pu**	94	239.0522	24,110	Fissile
^{240}**Pu**	94	240.0538	6,564	Fissionable

1.4.2 Neutron Interactions with Matter

When neutrons interact with matter, several reactions can occur generating a different result. These reactions include elastic scattering, inelastic scattering, radiative capture, charged-particle reactions, neutron producing reactions and fission. Elastic scattering takes place when a neutron collides with a nucleus and then continues on without transferring energy to the nucleus. In the inelastic scattering process, energy is

transferred to the nucleus by a neutron. Radiative capture occurs when a neutron is absorbed by the nucleus and one or more gamma rays are emitted. Charged particles including protons and alpha particles can be produced upon the capture of a neutron in the nucleus. A captured neutron can also produce successive neutrons released from the nucleus. In the fission process, a captured neutron causes a nucleus to split into two lighter nuclei (fission products).

For each type of neutron interaction (elastic scattering, inelastic scattering, radiative capture, charged particle or neutron producing reactions, and fission) involving a nucleus of a specific isotope, there exists a certain probability for which that process will occur. This probability is referred to as a microscopic cross-section σ. The macroscopic cross-section Σ is equal to the microscopic cross-section multiplied by the atom density of the isotope in question. Microscopic cross-sections are presented in units of either barns or cm^2 and macroscopic cross-sections are presented in units of cm^{-1}. The sum of all neutron interaction cross-sections provides the total cross-section representative of the probability that any neutron interaction will occur within an isotope.

Fission is one of the most significant neutron-induced processes used in nuclear engineering. Fission can occur in fissile and fissionable isotopes. Fissile isotopes possess a higher fission cross-section for low-energy neutrons and thus can fission from the capture of a thermal neutron that has an energy of 0.0253 eV. Fissionable isotopes possess a higher fission cross-section for fast neutrons. Thus, fissionable isotopes require a neutron of a prescribed critical energy above the binding energy in order to fission (where binding energy is the energy required to split a nucleus into its constituent nucleons). A notable example of the difference between fissile and fissionable isotopes is

the comparison of the fission cross-sections for fissile ^{235}U and fissionable ^{238}U as presented in Figure 1 (a) and (b). Fissile isotopes include special nuclear materials (SNM) such as ^{233}U, ^{235}U and ^{239}Pu. Fissionable isotopes include ^{234}U, ^{238}U and ^{240}Pu.

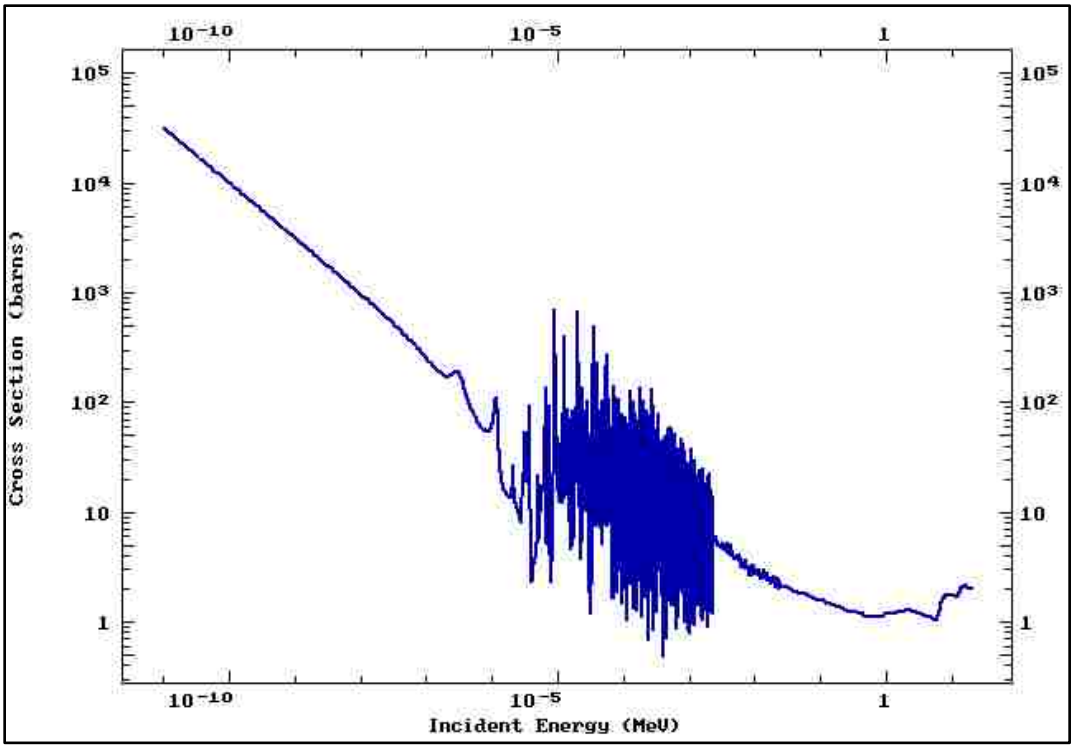

(a)

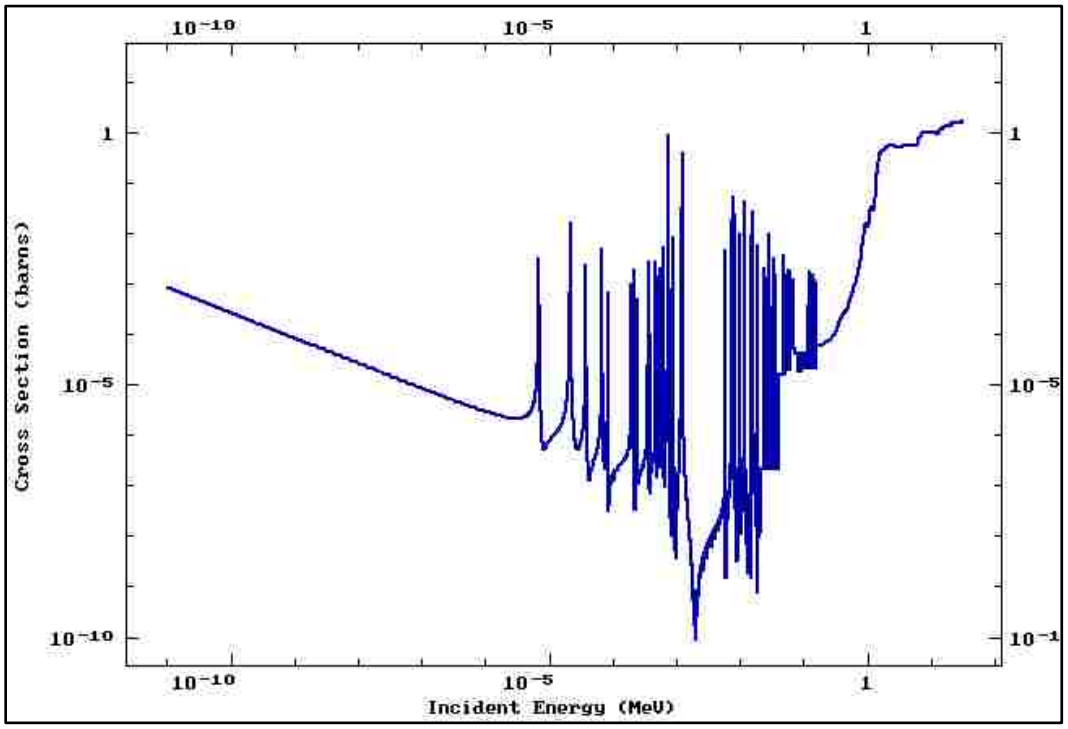

(b)

Figure 1 – Fission cross-sections for incident neutrons on (a) ^{235}U and (b) ^{238}U [3]

The liquid drop model describes the process of fission. It follows that an incident neutron is captured in a fissile / fissionable nucleus and the nucleus begins to oscillate developing a neck. The nucleus then splits into two lighter nuclei with smaller atomic numbers than the original nucleus. The fission product yield for the two lighter nuclei resulting from the splitting of ^{235}U is represented in Figure 2.

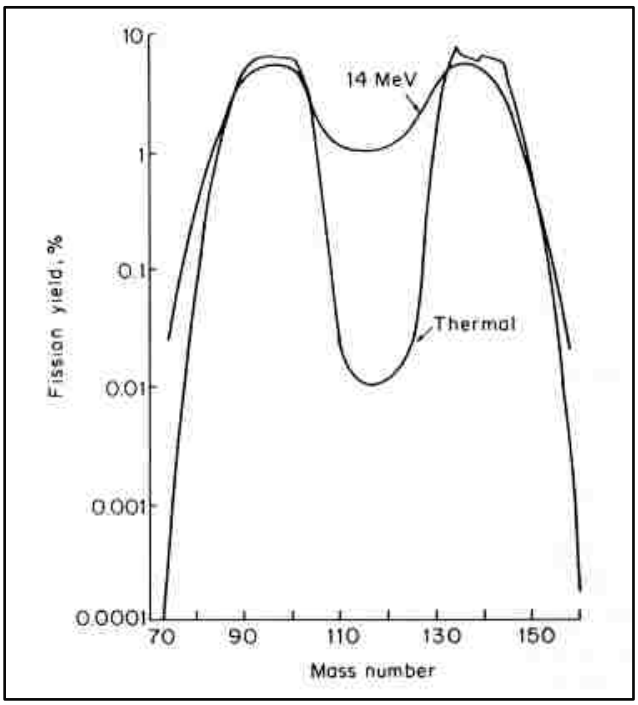

Figure 2 – Fission product yield from neutron-induced fission of ^{235}U [4]

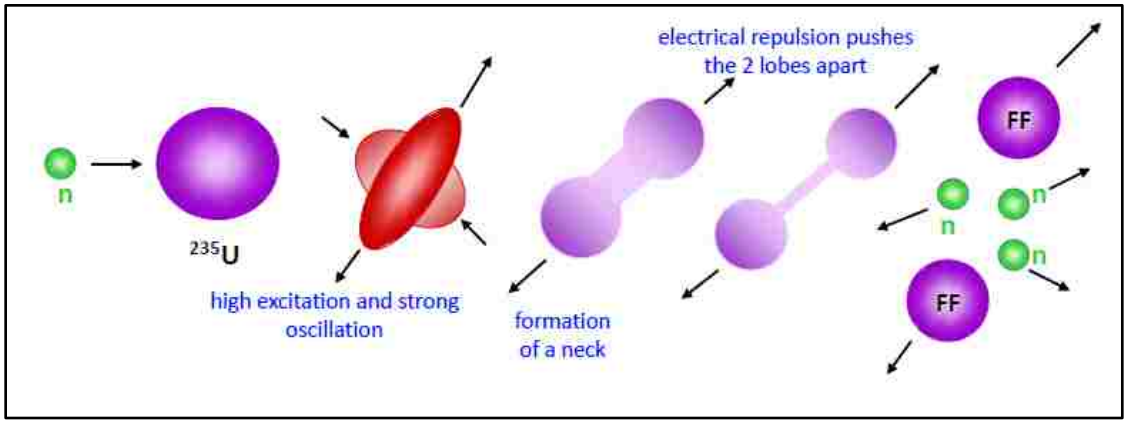

Figure 3 – Liquid drop model of fission process for ^{235}U

At the time of scission, prompt neutrons and gamma rays are released. On the order of milliseconds to seconds later, delayed neutrons and gamma rays are released. This process is illustrated in Figure 3. The resultant prompt and delayed neutrons and gamma rays make the detection of fissile and fissionable isotopes possible.

1.4.3 Gamma-Ray Interactions with Matter

As mentioned in the previous section, gamma rays can be produced by neutron interactions and importantly, gamma rays are created as a product of fission. Understanding how these resulting gamma rays interact with matter is essential to detecting them. The mechanisms in which gamma rays can interact with matter include the photoelectric effect, pair production and the Compton effect.

The photoelectric effect occurs when a photon is absorbed by the atom ejecting an electron from one of its bound shells (typically the K-shell). The probability for this interaction is described by the photoelectric cross-section. The photoelectron is emitted with an energy $E = h\nu - E_b$, where E_b is the binding energy of the electron in its atomic shell. In pair production, just as the name of this process indicates, an incident gamma ray on a nucleus disappears producing a pair of charged particles: one positron and one electron. This process is possible only if the photon energy exceeds twice the rest-mass energy of an electron (0.511 MeV). All photon energy in excess of 1.022 MeV is shared as the kinetic energy of the recoiling electron and positron. The probability that the pair production takes place in a nucleus is described as the pair production cross-section. The Compton effect occurs when an incident gamma ray scatters on the atomic electron of the absorber medium. The scattered gamma ray is deflected at an angle with respect to its

initial path transferring a fraction of its energy to the recoiling electron. The Compton effect cross-section describes the probability of this interaction.

1.4.4 Means of Detection

The detection of radiation such as neutrons and gamma rays has led to the discovery of new elements, the process of fission and fission chain reactions among many other outstanding discoveries in nuclear physics. Today, radiation detection technology serves as an essential component to improving national security and nonproliferation efforts. Detection methods have evolved tremendously over the last century to meet the changing needs of the nuclear enterprise.

Some of the common radiation detectors today include ionization chambers, proportional gas counters, Geiger-Mueller counters, semiconductor detectors and scintillation detectors. Each kind of instrument can detect different particles and electromagnetic waves. Instruments valuable to the detection of SNM are those which provide detection of neutrons and / or gamma rays. Two detectors used commonly for the detection of neutrons and gamma rays, respectively, are the ^{3}He gas proportional counter and the NaI(Tl) scintillation detector.

The NaI(Tl) crystal was first used as a gamma-ray detection scintillator in 1948 [5]. At the time, it produced a light output greater than ever seen before from any inorganic or organic scintillator. It is now used as the standard for all photon detectors and is a dominant scintillation material in the field of radiation detection. However, other scintillation detectors have since been discovered with improved detection characteristics. The effort to develop a scintillator with better gamma-ray detection characteristics continues today.

The ^{3}He gas proportional counter has long been utilized as a thermal neutron detector. Addition of a moderating medium such as polyethylene provides the ^{3}He detector the ability to detect fast neutrons. Unlike scintillators, ^{3}He counters detect neutrons via the nuclear reaction:

$$n + {}^{3}He \rightarrow p + {}^{3}H + 765\ keV\ [6] \qquad \textbf{(}\text{Equation 1}\textbf{)}$$

Subsequent proton and triton motion produces the ionization cloud of electron-ion pairs in the gas medium. The electrons and ions accelerate in the electric field of the counter thus generating a measurable electric signal. Although ^{3}He detectors have been a reliable means of neutron detection, the cost of ^{3}He gas is continually increasing with the decrease in resources. The natural abundance of ^{3}He gas on earth is only 0.000137% [7]. Thus, the majority of ^{3}He gas production comes from the decay of tritium. The dwindling volume of tritium production poses a risk to the continued growth of neutron detection technologies based on the ^{3}He isotope.

The desire to improve gamma-ray detector characteristics and the decrease in ^{3}He supply present a need for an easily manufactured, readily available, low cost neutron / gamma-ray detection alternative.

1.5 Scintillation Detectors

1.5.1 Mechanisms of Scintillation

Incident radiation interacts with a scintillator and produces detectable light (photons) proportional to the energy deposited in the scintillator. This light can then be detected by an optical readout unit such as a photomultiplier tube (PMT) and subsequently processed for analysis. All types of radiation produce light when interacting

with a scintillator, but the process of how the light is created differs for each material. When gamma rays interact with a scintillator either by the photoelectric effect, pair production or Compton scattering, electrons are produced that excite surrounding atoms. When these atoms de-excite, scintillation photons are emitted.

Fast neutrons interact with a scintillator by elastic scattering with hydrogen (protons) or carbon atoms. Elastic scattering with hydrogen is much more common. The imparted kinetic energy of the recoiling hydrogen or carbon atom is absorbed by the scintillator and scintillation photons are emitted.

For the case of thermal neutron interactions with a scintillator, the detectable light is created by yet another type of reaction. The ^{6}Li embedded in some scintillators is commonly used for the detection of thermal neutrons. The $^{6}Li(n,\alpha)^{3}H$ reaction has an energy Q-value of 4.78 MeV; a 2.05-MeV alpha particle and a 2.73-MeV triton are emitted. The charged particles excite the atoms of the scintillator thus producing detectable light.

1.5.2 Organic and Inorganic Scintillators

There exist two types of scintillating materials: organic and inorganic. The mechanisms for scintillation are different for organic and inorganic scintillators; however, the general scintillation process is the same.

Organic scintillators are generally composed of hydrogen and carbon atoms. Due to its low density and low atomic number, organic scintillators have been predominantly used as fast neutron detectors. Low cost and ease of fabrication make organic scintillators, specifically plastic scintillators, highly desirable, but at the cost of high

gamma-ray sensitivity. Prominent examples of organic scintillators include anthracene, plastics and liquids.

Inorganic scintillators exist in a multitude of materials, densities and atomic numbers. Inorganic scintillators are more commonly used in radiation detection applications than organic scintillators and are used principally for gamma-ray detection. These scintillators can be produced as pure inorganic materials; however, the addition of an activator is used to increase the detection efficiency. Detection characteristics of some inorganic scintillators can be superb to those of organic scintillators, but may have high cost or be difficult to fabricate. Widely used inorganic scintillators include sodium iodide (NaI), cesium iodide (CsI), bismuth germanium oxide (BGO) and lithium iodide (LiI).

1.5.3 Scintillation Detector Assembly

Whether an organic or an inorganic scintillator is used, the general components making up the scintillation detector assembly remain the same. As shown in Figure 4, scintillation detectors are commonly composed of a scintillation crystal, PMT and a high voltage divider, connected to a multichannel analyzer (MCA) and a computer. The scintillation crystal is optically coupled to the PMT. Light created in the scintillator produces electrons on the photocathode of the PMT. These electrons are accelerated by a strong electric field within the PMT. While the electrons accelerate, they collide with dynodes inside of the PMT and are multiplied. The resultant electrons produce an amplified output signal that is proportional to the energy of the incident radiation. The output signal is converted to a voltage waveform. This voltage signal is manipulated by a digitizer / MCA for comprehensible analysis by the user.

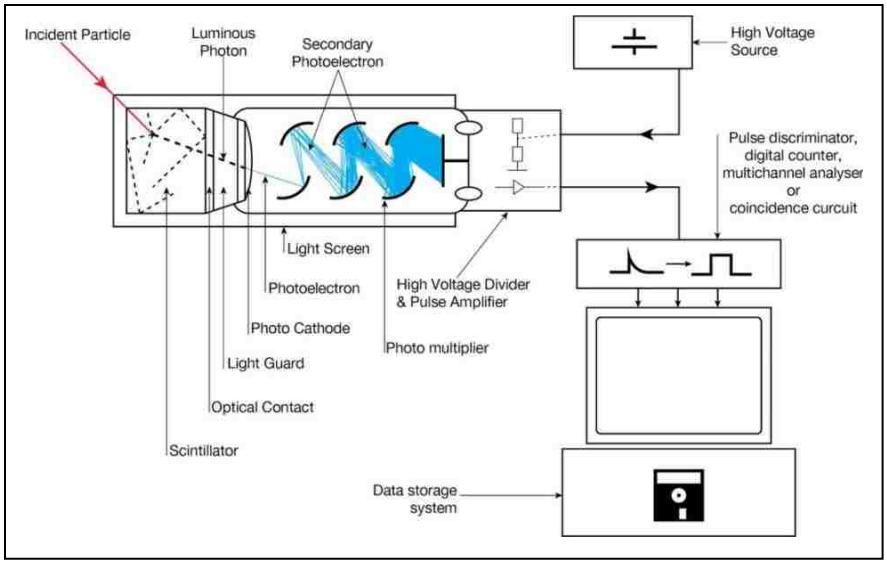

Figure 4 – Scintillation detector layout [8]

1.5.4 Characteristics of Scintillation Detectors

The performance of scintillation detectors can be characterized by several parameters. For gamma-ray and neutron detection, light yield (photons/MeV), energy resolution and decay time are significant. The figure of merit (FOM) parameter is utilized for the measurement of the detector's PSD performance. Light yield is a measure of the efficiency of a scintillator to convert the incident radiation to the light output and is presented in units of photons/MeV. The higher the light yield, the better the efficiency of the scintillator. Energy resolution of the detector is represented by the full width at the half maximum (FWHM) of a photopeak. Assuming a Gaussian function for a photopeak,

$$FWHM = 2\sigma\sqrt{ln2} \qquad \text{(Equation 2)}$$

where σ is the width parameter. The smaller the energy resolution or FWHM is, the higher the quality of detection results. The decay time characterizes the rate of energy loss of incident radiation on a scintillator. The decay time can differentiate particles for

PSD purposes as shown in Figure 5. The FOM is used to measure how well a scintillation detector can identify and separate different radiation particles. The FOM of a detector is determined with the following equation:

$$FOM = T/(W_1 + W_2) \qquad \text{(Equation 3)}$$

where T is the distance between the centroids of the peaks of particle 1 and particle 2, W_1 is the FWHM of the peak of particle 1 and W_2 is the FWHM of the peak of particle 2. This approach is illustrated in Figure 6.

Scintillation detectors continue to advance as the need to find a scintillator with optimum parameters continues. Low cost, high-resolution, sensitivity to both gamma rays and neutrons, good neutron / photon discrimination capabilities, ability to collect neutron and gamma-ray data simultaneously and the ability of directional detection all within a single scintillator are properties highly sought-after.

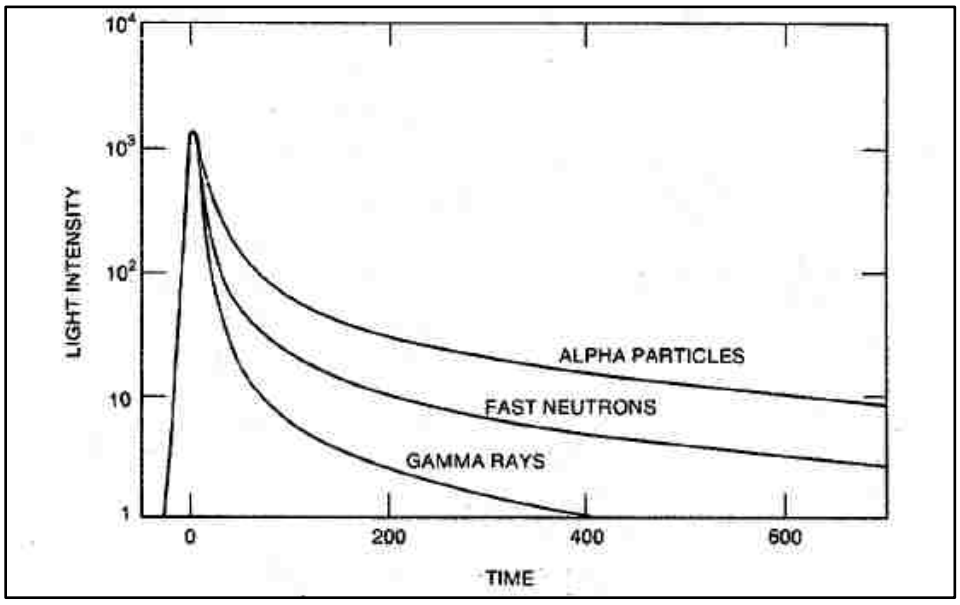

Figure 5 – Scintillation pulses for alpha particles, fast neutrons and photons in stilbene [9]

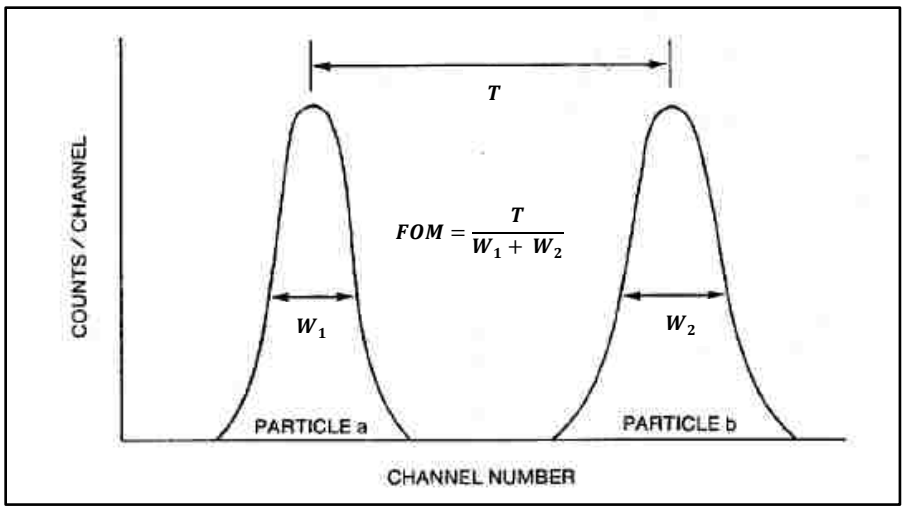

Figure 6 – Illustration of FOM [9]

CHAPTER 2

LITERATURE REVIEW

2.1 Review of Neutron and Photon Detection with Scintillators

An exceptional scintillator for neutron and gamma-ray detection requires several characteristics: high efficiency and proportionality in converting energy from incident radiation into fluorescence, transparency to its own fluorescence, a fast decay time, high resolution, and an index of refraction closely matching that of a photomultiplier tube (or other optical readout device) for efficient coupling. It is also important to consider which radiation particles are being detected; whether the particles are thermal neutrons, fast neutrons or gamma rays. For example, high atomic number or high density scintillators are ideal for gamma-ray detection as opposed to neutron detection for which hydrogenous materials with low atomic number and low density are ideal. There exists no single scintillator that possesses all of these characteristics; it is often a compromise between one characteristic and another.

The evolution of scintillators for neutron and gamma-ray detection has been an enduring effort to investigate organic and inorganic materials alike in search of an optimum scintillator. Many scintillating materials have been studied, but few have stood out among the rest. Some of the most notable and widely used scintillators include thallium-activated sodium iodide (NaI(Tl)), thallium- and sodium-activated cesium iodide (CsI(Tl) and CsI(Na)), bismuth germanium oxide (BGO), europium-activated lithium iodide (LiI(Eu)) and plastic scintillators. All of these scintillators have been studied thoroughly, commercially produced and applied successfully in the field.

2.1.1 Thallium-Activated Sodium Iodide NaI(Tl)

The NaI(Tl) scintillator was first studied in 1948 by Robert Hofstadter and yielded an impressively large scintillation light output [5]. At that time, the light output produced by NaI(Tl) trumped that of previously studied scintillators. It is known as the "gold standard" of gamma-ray scintillators and remains a highly competitive and widely used scintillation detector today. It possesses an absolute light yield of 38,000 photons/MeV and a scintillation decay time of 0.23 μs [5].

2.1.2 Cesium Iodide (CsI)

The CsI(Tl) scintillator has gained much interest due to its even higher absolute light yield and robust nature. The absolute light yield of CsI(Tl) is 65,000 photons/MeV and its scintillation decay time is 0.68 μs [5]. The absolute light yield of CsI(Na) is 39,000 photons/MeV and its scintillation decay time is 0.46 μs [10].

2.1.3 Bismuth Germanium Oxide (BGO)

Bismuth germanium oxide, or BGO for short, is a gamma-ray scintillator more recently developed than NaI(Tl) and CsI. Although its scintillation properties appear somewhat inferior to NaI(Tl) and CsI(Tl) or CsI(Na), this scintillator has a high density of 7.13 g/cm^3 and a large atomic number of 83 from bismuth. These desirable properties result in a higher probability for the photoelectric absorption of gamma rays [5]. The BGO scintillator possesses a refractive index of 2.15, a decay time of 0.30 μs and an absolute light yield of 8,200 photons/MeV. The high refractive index and the low light yield limit the applicability of this scintillator.

2.1.4 Europium-Activated Lithium Iodide (LiI(Eu))

The inorganic scintillator LiI(Eu) is widely used as a thermal neutron scintillator due to its chemical similarities to thallium-activated sodium iodide (NaI(Tl)) and its ability to detect thermal neutrons. Due to the unique signal produced by the capture of thermal neutrons on ^{6}Li, discrimination between thermal neutrons and gamma rays can be performed. It has a decay time of 1.4 μs and an absolute light yield of 11,000 photons/MeV.

2.1.5 Plastic Scintillators

Organic plastic scintillators can be used for the detection of thermal neutrons, fast neutrons and gamma rays. Plastic scintillators of different material compositions are capable of detecting different radiation particles. Companies including Saint Gobain Corporation and Eljen Technology produce a variety of these organic detection mediums as low cost alternatives for radiation detection.

The Saint Gobain Corporation produces plastic scintillators for the application of thermal neutron, fast neutron and gamma-ray detection. Scintillators capable of thermal and fast neutron detection are among the most notable scintillators produced by Saint Gobain. The boron-loaded BC-454 plastic scintillator is used for the detection of thermal neutrons. This scintillator possesses a decay constant of 2.2 ns and a light output of 48% anthracene [5]. The BC-436 plastic scintillator contains deuterated styrene in which fast neutrons can be detected. This plastic scintillator possesses a light output of 52% anthracene and scintillation decay time of approximately 2.2 ns [11].

Eljen Technology produces plastic scintillators comparable to those produced by Saint Gobain Corporation. One of the newest scintillators produced by Eljen Technology

is the EJ-299-33 plastic scintillator to which there exists no Saint Gobain counterpart. This scintillator can be used for the detection of fast neutrons and is capable of gamma-ray and fast neutron discrimination. It possesses a light output of 56% anthracene [12]. No scintillation decay time is specified by Eljen Technology for the EJ-299-33 plastic scintillator.

2.2 Review of Elpasolite Scintillators

A newly evolving group of cerium-activated fast inorganic materials known as elpasolites has shown encouraging scintillating performance capable of gamma-ray and neutron detection simultaneously. The unique name elpasolite comes from a naturally occurring mineral originally found in El Paso County, Colorado [5]. Elpasolites have the general formula $A^{+}B^{+}B'^{3+}X^{-}$ where A^{+} and B^{+} are most often alkali metals, B'^{3+} is a rare-earth metal, transition metal, or other trivalent ion, and X^{-} is a halogen ion [13]. Many elpasolites also contain cerium as an activator.

Several elpasolite materials have been studied, investigating each scintillator's gamma-ray energy resolution, decay time, absolute light yield and pulse shape discrimination capabilities. These elpasolites include Cs_2LiYCl_6:Ce (CLYC), $Cs_2LiLaCl_6$:Ce (CLLC), $Cs_2LiLaBr_6$:Ce (CLLB), and Cs_2LiYBr_6:Ce (CLYB) among many others.

A great amount of attention and effort has been invested in CLYC due to its excellent pulse shape discrimination capabilities; it has been reported that there is only one gamma ray per 1000 that triggers a neutron false positive [14]. This material contains cesium (Cs), lithium (Li), yttrium (Y), chlorine (Cl) and is doped with cerium (Ce). Its physical form is a clear crystal [15]. The size of the CLYC crystal is significantly limited

due to non-congruent melting when growing the crystal. This causes cracks, bubbles and inclusions in the crystal. A cylindrical crystal of 1-inch-diameter and 1-inch-height has been successfully developed without bubbles, cracks or inclusions. Cylindrical CLYC crystals with dimensions of 2-inch by 2-inch and 3-inch by 3-inch are still developing these defects and are currently being improved [15]. This elpasolite provides the ability to measure photon and neutron data simultaneously. Immaculate pulse shape discrimination and directional detection capabilities are possible with CLYC. It is these characteristics which make CLYC a desirable candidate for a dual neutron / gamma-ray directional detection system.

The following is a synopsis of the work on CLYC performed by three institutions: Delft University of Technology, Radiation Monitoring Devices, Inc., and the NSTec Remote Sensing Laboratory. The information gained from these experiments has contributed a great deal to the knowledge and progress of CLYC.

2.2.1 Delft University of Technology

The CLYC crystal was first discovered, developed and studied at the Delft University of Technology in the Netherlands in 1999 [16]. It was, at the time, considered as an excellent candidate for the detection of thermal neutrons. CLYC contains lithium and thus possesses the ability to produce detectable scintillations via the following reaction:

$$ {}^{6}_{3}Li + {}^{1}_{0}n \rightarrow {}^{3}_{1}H + \alpha \qquad \text{(Equation 4)} $$

An incident thermal neutron on a ^{6}Li atom produces two ionizing particles: a triton and an alpha particle that share the kinetic energy. These ionizing particles produce scintillations within the CLYC crystal.

Multiple elpasolites were studied, but CLYC reigned supreme. The properties of both pure CLYC and Ce^{3+}-doped CLYC were studied. The crystals were grown using the vertical Bridgman method to a size of approximately $3\times3\times4$ mm^3. The x-ray excited emission spectra, pulse-height spectra and scintillation decay measurements were performed in the initial experiment. The x-ray excited emission spectra provided evidence that the Ce^{3+}-doped CLYC crystal yielded a much higher photon yield than the undoped CLYC crystal. The addition of Ce^{3+} produced a photon yield nine times higher. Pulse-height measurements reflected the response of the Ce^{3+}-doped CLYC crystal to ^{137}Cs radiation with the characteristic gamma-ray peak at 662 keV. The energy resolution found at this peak was stated to be approximately 7.3%. The corresponding photon yield was found to be 20,000 photons/MeV. The scintillation decay measurements yielded a decay time for the Ce^{3+}-doped CLYC crystal of 600 ns.

These results showed much promise for the Ce^{3+}-doped CLYC crystal as a thermal neutron scintillator. However, it was hypothesized that even though CLYC possessed a higher photon yield in comparison to LiI(Eu) (a more commonly accepted thermal neutron scintillator), the CLYC would perform inferiorly to LiI(Eu) for pulse shape discrimination purposes due to its lower lithium content. This hypothesis was later found to be false.

The Delft University of Technology revisited the pulse shape discrimination capabilities and other gamma-ray and neutron detection properties of CLYC in 2004 [17].

As in the first experiment, a 3×3×4 mm^3 Ce^{+3}-doped CLYC crystal was used. This crystal was sealed inside of a quartz housing wrapped in Teflon tape and coupled via a coupling fluid to a Phillips XP2020Q photomultiplier tube. The CLYC detector was then exposed to radiation emitted from a ^{137}Cs source. The results yielded from this experiment agreed well with the 1999 experiment. The photon yield observed was slightly increased to 21,600 photons/MeV. However, the characteristic gamma-ray peak of ^{137}Cs at 662 keV was observed with a lower resolution of 8.0%. The thermal neutron peak appearing above 3.0 MeV gamma-ray equivalent energy (GEE) possessed a resolution of 5.5%. This thermal neutron characteristic had not yet been investigated by the Delft University of Technology. The scintillation pulse-height spectrum providing the aforementioned gamma-ray and thermal neutron peaks is provided in Figure 7. The pulse shape discrimination capabilities of the CLYC crystal appeared to be much more promising in the 2004 results as opposed to the 1999 results. The scintillation pulses created in the CLYC detector were measured using a digital oscilloscope. When irradiated by ^{137}Cs, the results showed a fast component in the time dependence of the scintillation pulses, which was determined to be a product of the core-to-valence luminescence (CVL). The CVL was not observed when the CLYC detector was exposed to a thermal neutron flux. The presence of the CVL during the gamma-ray excitation and the absence of it during the thermal neutron excitation indicated that excellent pulse shape discrimination was possible. It was this observation at the Delft University of Technology which gave rise to a larger interest in studying the CLYC crystal. Radiation Monitoring Devices, Inc. would soon take a great interest in these results and would further investigate what photon / neutron detection possibilities the CLYC crystal held.

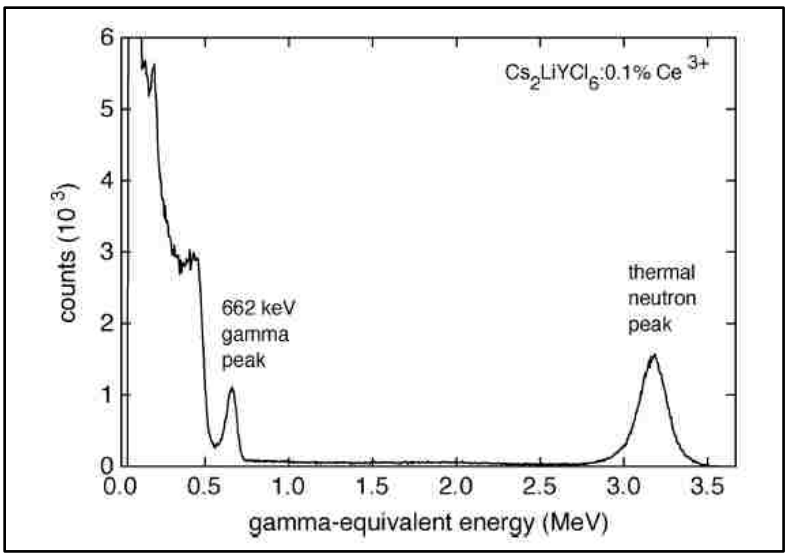

Figure 7 – Scintillation pulse-height spectrum of CLYC exposed to gamma rays of ^{137}Cs and thermal neutrons [17]

2.2.2 Radiation Monitoring Devices, Inc.

Established in 1974, Radiation Monitoring Devices, Inc. (RMD) exists as a hub for radiation detection technologies research in the United States. Keeping in mind the increasing importance of homeland security and nonproliferation efforts, RMD has made significant developments towards achieving a successful dual gamma-ray / neutron detector by utilizing the elpasolite CLYC. Building on the achievements made by the researchers at the Delft University of Technology with smaller CLYC crystals, RMD, Inc. developed a 1-inch-diameter CLYC crystal in 2008 for which its properties were examined [18]. This crystal was grown utilizing the Bridgman method. The constituents of the crystal were mixed together and melted in a furnace. The resulting 3.3 g/cm^3 dense CLYC crystal was then cooled and encapsulated within a housing with a quartz window so to prevent degradation to the crystal.

Several important characteristics of the CLYC crystal were investigated in this study including gamma-ray energy resolution, neutron detection and PSD performance.

The energy spectra were measured by coupling the 1-inch-diameter CLYC crystal to a Hamamatsu R6233 PMT using optical grease. The PMT was then connected to a 2005 Canberra preamplifier, which in turn was connected to a spectroscopy amplifier and a multichannel analyzer (MCA). The energy spectra produced by the CLYC detector when exposed to ^{137}Cs was evaluated and compared to that produced by a NaI detector. The CLYC detector produced an energy resolution of 5.1% ± 0.1 for the ^{137}Cs 662-keV gamma-ray full energy peak. The NaI detector produced an energy resolution of 7.2% ± 0.1 for the ^{137}Cs 662-keV gamma-ray full energy peak. The comparison of the CLYC and NaI detector responses are graphically represented in Figure 8. These intriguing results provoked further research of the CLYC as a gamma-ray detector.

The neutron detection performance was then investigated using the same CLYC detector system. The CLYC detector was exposed to a ^{252}Cf source. As shown in Figure 9, the neutron peak is easily distinguishable from the gamma-ray part of the energy spectrum. The 3.2 MeV gamma-ray energy equivalent neutron peak of ^{252}Cf possesses an energy resolution of 2.9%. A digital scope was then attached to the PMT and provided time profiles of gamma-ray and neutron excitations within the CLYC scintillator. These time profiles, Figure 10, demonstrate a fast rise time and decay for gamma-ray excitation and a slower rise time and decay for neutron excitation. These results demonstrate that PSD can be achieved with the CLYC crystal.

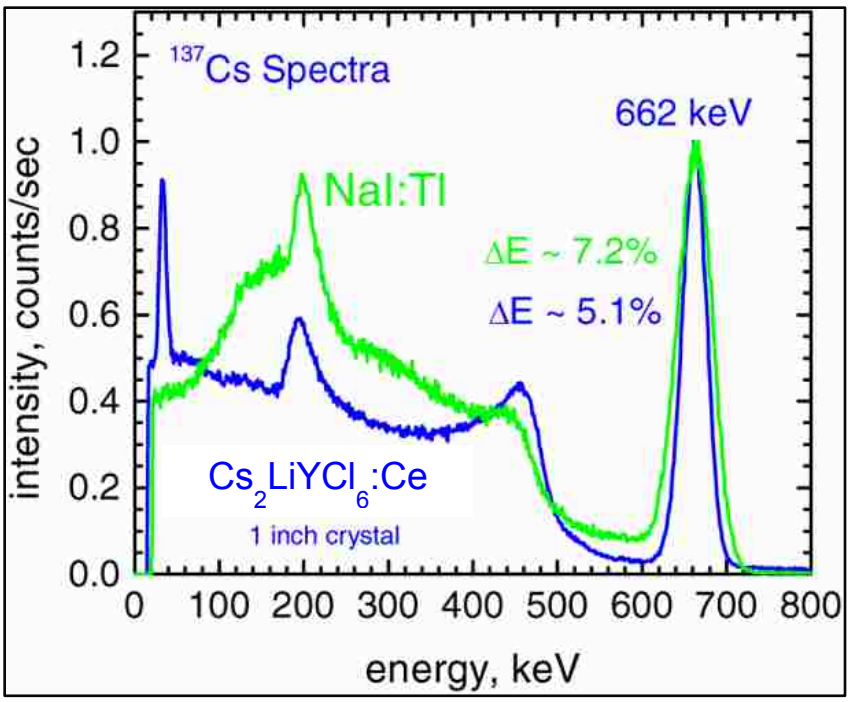

Figure 8 – Gamma-ray responses of CLYC versus NaI(Tl) detectors [18]

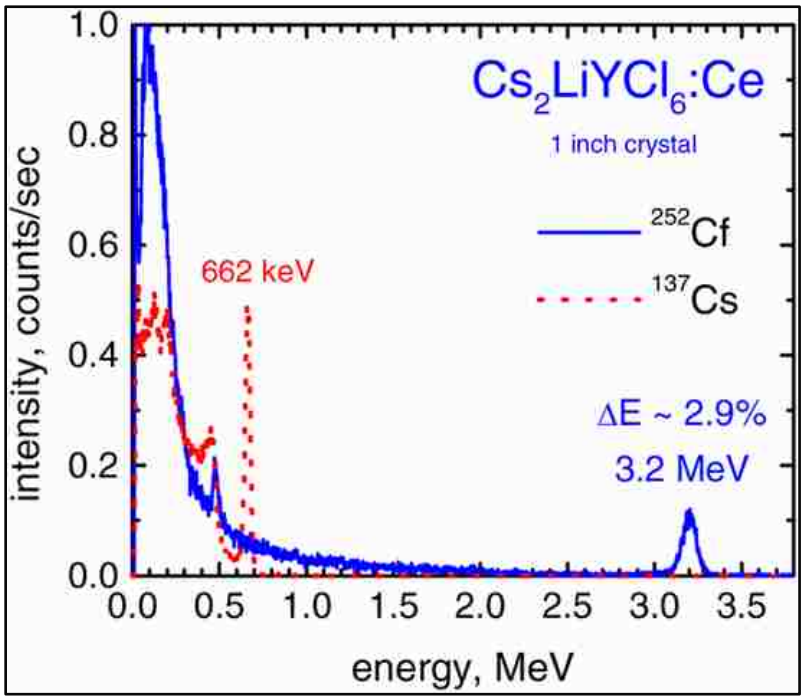

Figure 9 – Gamma-ray / neutron response of CLYC [18]

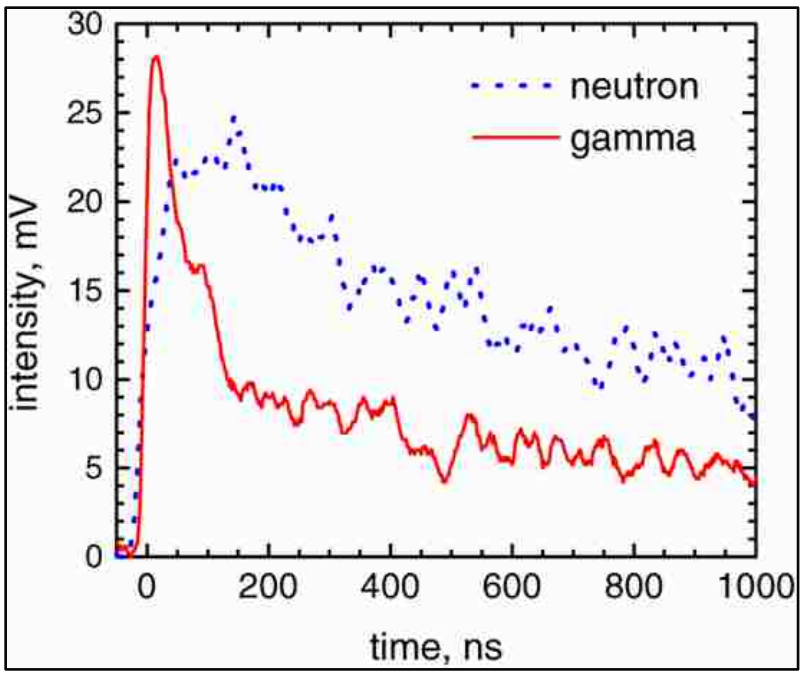

Figure 10 – Time profiles for PSD of CLYC [18]

This first experiment by RMD, Inc. provided motivation for further CLYC research and development. Between 2008 and 2012, RMD, Inc. produced several publications demonstrating their successes with CLYC as a dual gamma-ray / neutron detector [18, 14, 19, 20, 21]. This collection of publications presents the best values achieved by RMD, Inc. for gamma-ray and neutron detection characteristics for the CLYC scintillator. Latter experiments with the CLYC scintillator yielded increasingly impressive results producing a photon yield of 20,000 photons/MeV, a gamma-ray energy resolution of 3.9% and a decay time of 55 ns. These experiments continued to yield a gamma-ray equivalent energy for neutrons of 3.2 MeV with an energy resolution of 2.9% and excellent pulse shape discrimination results.

2.2.3 NSTec Remote Sensing Laboratory

The Remote Sensing Laboratory (RSL) is located on the Nellis Air Force Base in Las Vegas, NV, and is operated by National Security Technologies, LLC (NSTec), for the U.S. Department of Energy, National Nuclear Security Administration. The focus of the RSL mission is to develop and implement advances in remote sensing technologies in support of radiological emergency response and nonproliferation. As part of a continuous effort to improve remote sensing technologies, the RSL has invested a great interest in the CLYC as a dual gamma-ray / neutron directional detector. The RSL studied the previous experiments and results published by the Delft University of Technology and RMD on the CLYC crystal as a scintillator for radiation detection. The discoveries from these experiments served as the foundation for the RSL's own research on the CLYC elpasolite. The RSL team proposed several tasks to complete in investigating the performance of CLYC. The first task included the modeling of the CLYC's directional detection capabilities. This was accomplished via the Monte Carlo particle transport code MCNPX developed at Los Alamos National Laboratory. Predictive models of an array of three and an array of four CLYC detectors exposed to a gamma-ray radiation source were simulated in MCNPX. The count rate as a function of angle was calculated. These results indicated that an array of three or four CLYC detectors could indeed perform directional detection of radioactive sources [22]. The second task was to perform sensitivity analyses of CLYC as a dual neutron / gamma-ray detector using physical experiments. A 1-inch-diameter and 1-inch-height CLYC crystal was acquired by the RSL from RMD. The CLYC crystal was then optically coupled to a Hamamatsu Super Bialkali (SBA) R6231-100 PMT. The CLYC crystal and the PMT were encapsulated together so to prevent

ambient light from interfering with the detection results. When exposed to ^{137}Cs, the CLYC detector yielded a 5% resolution for the 662-keV characteristic gamma-ray peak. When exposed to ^{252}Cf, the CLYC detector yielded a 3.4% resolution of the ^{6}Li thermal neutron capture peak, which appeared at approximately 3.0 MeV gamma-ray equivalent energy [23]. These results agreed well with existing CLYC research and it was hypothesized that even better results could be achieved by RSL.

In addition to the two aforementioned completed tasks, several tasks remained to be executed. These tasks included neutron / gamma-ray pulse shape discrimination evaluations, fabrication and benchmarking, testing and characterization of an array of multiple CLYC detectors for directional detection.

2.3 Review of Directional Radiation Measurements

For applications where the location of a radioactive source is unknown, directional radiation detectors are vital to the search and localization of these sources. There exist several directional radiation detection systems that utilize different detecting materials and different means of integrating the collected data. However, these systems share the same purpose: to detect, find and identify radiation sources. Several applications of directional radiation detection systems include detection of radioactive sources in urban locations and at large events, remote sensing for sources or contamination and the aid of search teams in the recovery of orphaned sources.

Four directional radiation detection systems will be discussed. Each system is unique, utilizing different detection materials, mathematical algorithms and overall system design. The components, capabilities and other pertinent details are highlighted in the following review.

2.3.1 Intelligent Radiation Sensor System

The U.S. Domestic Nuclear Detection Office (DNDO) issued a challenge for companies to develop a low cost, portable directional radiation detection system for the purposes of homeland security applications. Passport Systems, Inc. developed a prototype system winning this challenge. The system is named the Intelligent Radiation Sensor System (IRSS) and consists of a network of portable radiation detectors from which data is gathered and fused together providing information on the detection, localization and identification of radioactive threats [24].

This system includes several key components (see Figures 11 and 12). A network of individual radiation detection devices (IRDD) collects data on the radioactive source in question. These IRDDs are made up of a NaI(Tl) detector with PMT and subsequent electronics. The data collected from these IRDDs is transmitted via WiFi to a detector augmentation device (DAD). The DAD interfaces with the IRDDs through Android smartphone technology. It also acts as the main communication and computation center for the IRSS. The DAD contains all of the mathematical algorithms required for detection, localization and identification of a radioactive source.

There are two algorithms utilized in the IRSS. The first algorithm is used for background radiation estimation. The execution of this algorithm prevents false positives produced from background radiation by estimating the activity levels of that background radiation. The second algorithm utilized by the IRSS is for source estimation. This algorithm is a peak-finding and peak-matching algorithm based on a sampled Bayesian inference method. It allows the user of the IRSS to detect and localize a radioactive source.

The IRSS prototype was completed and submitted to the DNDO on June 1, 2012. It includes 44 prototype detection devices, a wireless mesh network, a reach-back network and one base control unit. Analysis of data gathered at the Savannah River National Laboratory by the IRSS is currently taking place.

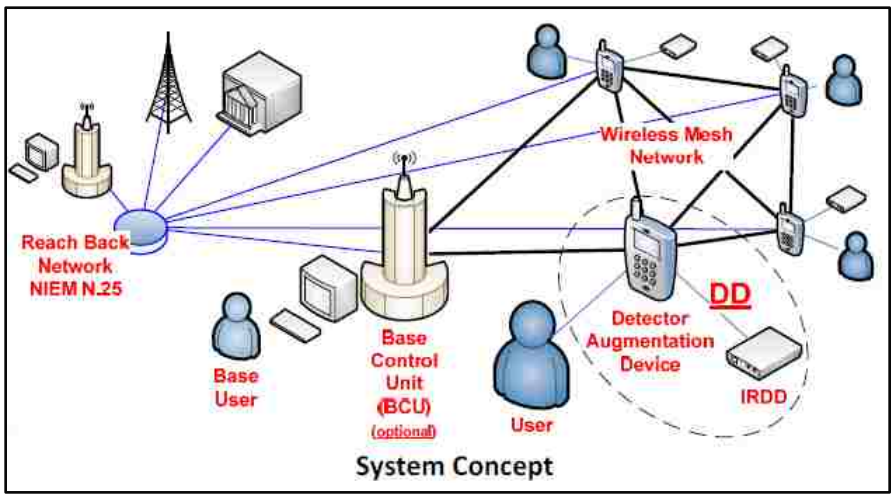

Figure 11 – IRSS detection network [24]

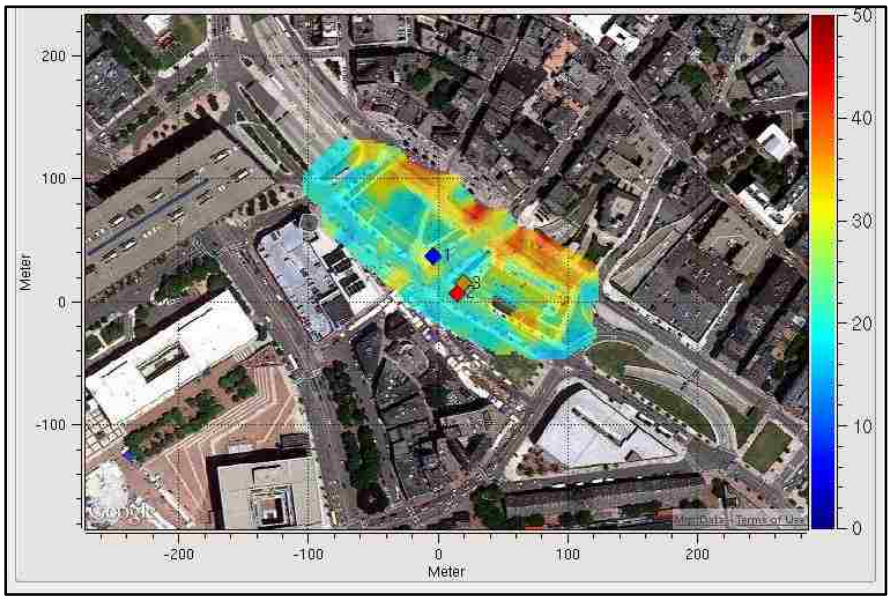

Figure 12 – NORM background measurements using three IRSS networked detectors on the Rose Kennedy Greenway Park in Boston, MA [24]

2.3.2 Integrated Directional / Non-Directional Detector System

Collaborators Budhaditya Deb, J. A. Fergus Ross, Adrian Ivan, and Michael J. Hartman developed a system of non-directional and directional detectors for the purposes of estimating the activity and location of a radioactive source [25]. This detector system combines data from both non-directional detectors and directional detectors via maximum likelihood algorithms providing the user of the system information pertinent to locating and identifying a radioactive source.

Two different detection materials and algorithms are used for the non-directional detectors and the directional detectors. The non-directional detectors consist of scintillators of undisclosed materials. The data gathered from these non-directional scintillation detectors is interpreted via a maximum likelihood estimation algorithm with which the radioactive source parameters are estimated. The directional detector consists of a CZT-based Compton detector. The data gathered from the directional detectors is interpreted via a maximum likelihood expectation algorithm and is used to locate the source in a Cartesian coordinate system. The fusion of information from both non-directional and directional detectors and both maximum likelihood algorithms provides a reasonable estimate of the activity and location of a radioactive source.

This detector system does possess several significant limits. The first limitation is that the radiation background levels in a given location must already be known prior to use of this system. The second limitation is that the system can only detect one radioactive source at a time.

The principal focus during the development of this detector system was to create a successful fusion of maximum likelihood algorithms so to integrate the information

gathered concerning the radioactive source from both the non-directional and the directional detectors. So despite the limitations of the system, the collaborators were able to successfully implement the aforementioned algorithms and furthermore, integrate the information provided by both the non-directional detectors and the directional detectors so to estimate the location and activity of a radioactive source.

2.3.3 3-D Plastic Scintillator Detector Array

The All-Russia Research Institute of Automatics in Moscow, Russia utilized the capabilities of an array of plastic scintillators for the purposes of directional radiation detection [26]. The 3-D detection array gathers the arrival time, spatial coordinates and amplitude of a scintillation signal occurring in any detector of the array. From this information, neutron and gamma-ray sources can be identified and localized. Furthermore, this system is capable of neutron / gamma-ray discrimination, radiation source imaging and reducing the interference from background radiation.

This 3-D detection array consists of several plastic scintillators coupled to photo receivers. Subsequent electronics and a system of wavelength shifting fibers manipulate the collected signals into an analyzable form. Two methods of localizing a radioactive source with this detection system have been tested and determined to be successful. The first method is by evaluating the spatial distribution of the incident radiation. The second method is by studying the neutron / gamma-ray scattering kinematics.

The success of this 3-D detection array is due to its capabilities to identify a radiation source, determine the direction towards the source, determining the activity of the source, performance of neutron / gamma-ray discrimination and background radiation rejection. Further improvements to this detector system are currently being pursued.

2.3.4 Tandem Directional Detector

The National Institute of Radiological Sciences in Japan has developed a directional radiation detector utilizing two scintillators in series [27]. It is suggested by the authors that placing two different scintillators in tandem increases the directional sensitivity to gamma rays. This tandem directional detector is designed to measure the direction, energy and count of incident gamma rays. This directional detection system has been used to locate orphaned radioactive sources and radioactive contamination.

The commonly used NaI(Tl) and BGO scintillators constitute the detection material of this system. The NaI(Tl) scintillator is coupled to the BGO scintillator, which is coupled to a photomultiplier tube. Subsequent electronics amplify the scintillation signals to be analyzed. An array of three tandem directional detectors comprises this detection system. The relationship between gamma-ray interaction position in the NaI(Tl) scintillator with the position in the BGO scintillator provides the directionality of the radioactive source being detected. This relationship is described via the equation:

$$R = \frac{Photopeak\ counts\ by\ NaI(Tl)\ scintillator}{Photopeak\ counts\ by\ BGO\ scintillator} \qquad \text{(Equation 5)}$$

This system has been thoroughly tested and has provided practical results for field applications. The utilization of the NaI(Tl) and BGO scintillators coupled with the mathematical relationships of a tandem detector has provided this directional detection system with the ability to successfully detect and localize a gamma-ray source.

CHAPTER 3

EXPERIMENTAL STUDY

3.1 Dual Neutron / Photon Detector System

3.1.1 Scintillator

The examined scintillator is a Cs_2LiYCl_6:Ce (CLYC) crystal produced by RMD, Inc. [28]. The CLYC scintillator has proven to demonstrate a gamma-ray energy resolution at 662 keV of less than 5%. In Figure 13, it is presented that the CLYC scintillator achieves a gamma-ray energy resolution at 662 keV of 4.3%. This energy resolution is 25 – 30% better than a typical NaI gamma-ray scintillator. The energy resolution of the thermal neutron peak appearing at approximately 3.2 MeV gamma-ray equivalent energy (GEE) is 2.5% as presented in Figure 13. The thermal neutron cross-section of ^{6}Li present in CLYC is 940 barns. The cross-section of ^{6}Li is 2.3 times higher than ^{3}He at 10 atm as suggested by Figure 14. The higher the total neutron cross-section is, the higher the probability that a neutron will interact with the target material (in this case the CLYC crystal). PSD is utilized to easily separate gamma-rays and neutrons detected within the CLYC scintillator. The CLYC emission consists of three components [22]. The first two components to appear are due to gamma-ray interaction in the scintillator and include core-to-valence (CVL) luminescence and Ce^{3+} emission. The third component appears due to thermal neutron interaction within the CLYC and is due to cerium self-trapped excitation (Ce-STE). The significant difference in the decay times of the gamma-ray versus neutron-induced emission components allow for excellent PSD capabilities. PSD utilizing data performed by RMD, Inc. utilizing an americium-beryllium (AmBe) source is presented in Figure 15.

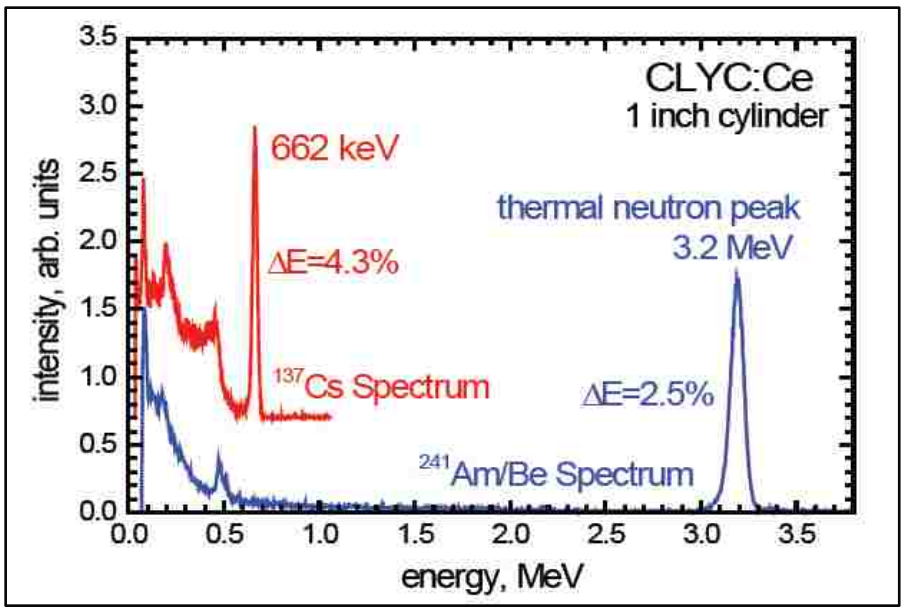

Figure 13 – CLYC gamma-ray and neutron energy spectra [28]

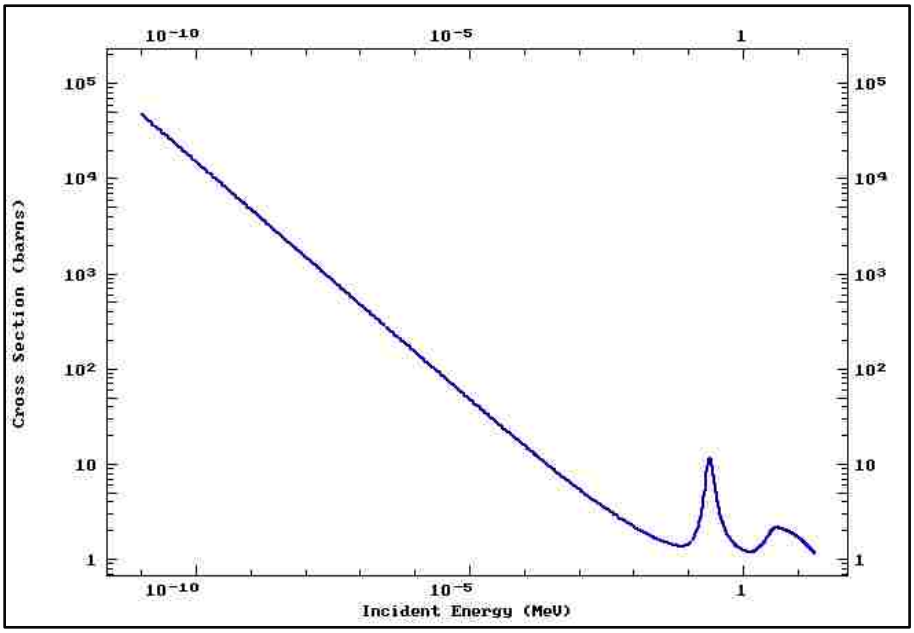

Figure 14 – Total neutron cross-section for ^{6}Li [3]

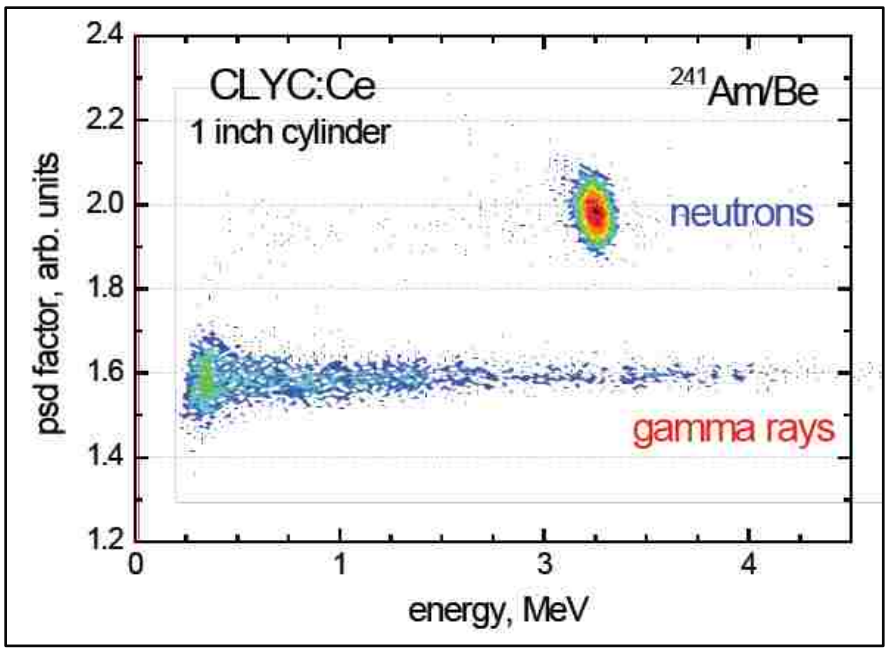

Figure 15 – CLYC pulse shape discrimination [28]

The 1-inch-diameter, 1-inch-height CLYC crystal is hermetically sealed to prevent damage to the crystal. There is a quartz optical window on one end of the encapsulated crystal for coupling to a PMT. The encapsulated CLYC crystal used for this study is shown in Figure 16. Some of the properties pertinent to the application of the CLYC as a dual neutron / gamma-ray detector are presented in Table 3.

Figure 16 – Encapsulated 1-inch CLYC crystal used in experiments

Table 3 – Properties of the CLYC scintillator [28]

Property	Value
Material	Cs_2LiYCl_6:Ce
Melting Point	640 °C
Density	3.31 g/cm^3
Water Solubility	Hygroscopic
Refractive Index	1.810±0.037 @ 405 nm
Emission Spectral Range	275 – 450 nm
Peak Scintillation Wavelength	370 nm
Decay Constants (CVL, Ce^{3+},Ce-STE)	1 ns, 50 ns, 1000 ns
Scintillation Light Yield (photons)	20,000 photons/MeV
Scintillation Light Yield (neutrons)	70,000 photons/neutron
Gamma-ray Energy Resolution @ 662 keV	4.3%
Thermal Neutron Energy Resolution @ 3.2 MeV GEE	2.5%

3.1.2 Optical Readout Subsystems

The optical window of the aforementioned encapsulated CLYC crystal is coupled to a photomultiplier tube using the Saint-Gobain Crystals silicone grease BC-630. For preliminary measurements before the aluminum detector housing was completed, the CLYC crystal was coupled to an 8-stage Hamamatsu R6231-100-01HA PMT and assembled into a temporary detector housing [29]. The R6231-100-01HA PMT is presented in Figure 17 (a). This PMT measures 51 mm in diameter with an effective diameter of 46 mm. The spectral response of this PMT is 300 to 650 nm, peaking at 350 nm. It is a head-on type PMT meaning the photocathode is formed directly on to the inner surface of the optical window of the PMT allowing for easy coupling of scintillators. The

photocathodes are super bialkali (SBA) type having a moderately high quantum efficiency of 35% at the peak wavelength of 350 nm [30]. Other important properties of the Hamamatsu R6231-100-01HA PMT are included in Table 4.

Once the aluminum detector housing was completed, the encapsulated CLYC crystal was optically coupled to a smaller 9-stage PMT and assembled within the final detector housing. The PMT used was the Hamamatsu R3998-100-02HA pictured in Figure 17 (b).

Table 4 – Properties of the Hamamatsu R6231-100-01HA PMT [30]

Property	Value
Dynode Stages	8
[Max. Rating] Anode to Cathode Voltage	1500 V
[Max. Rating] Average Anode Current	0.1 mA
Anode to Cathode Supply Voltage	1000 V
[Cathode] Luminous Sensitivity Min.	110 μA/lm
[Cathode] Luminous Sensitivity Typ.	135 μA/lm
[Cathode] Blue Sensitivity Index (CS 5-58) Typ.	13.5
[Cathode] Radiant Sensitivity Typ.	110 mA/W
[Anode] Luminous Sensitivity Min.	3 A/lm
[Anode] Luminous Sensitivity Typ.	30 A/lm
[Anode] Radiant Sensitivity Typ.	2.5×10^4 A/W
[Anode] Gain Typ.	2.3×10^5
[Time Response] Rise Time Typ.	8.5 ns
[Time Response] Transit Time Typ.	48 ns

(a) **(b)**

Figure 17 – (a) R6231-100-01HA 51-mm PMT; (b) R3998-100-02HA 25-mm PMT

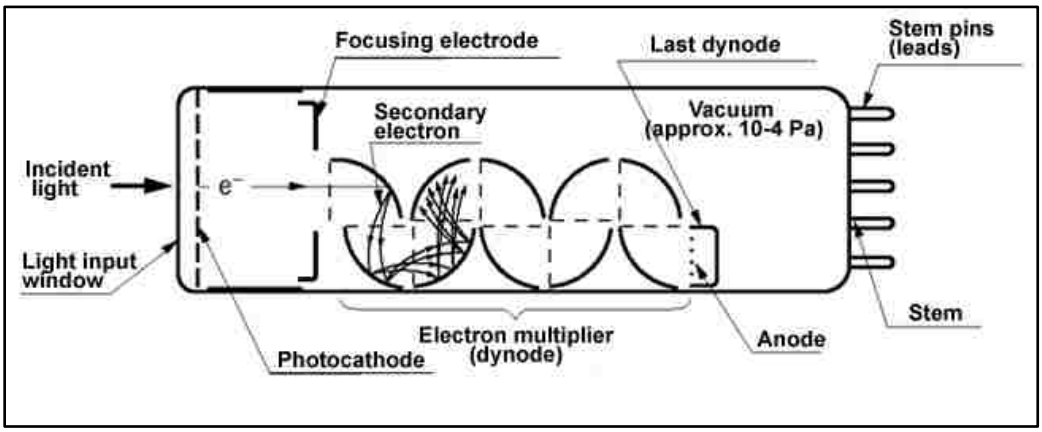

Figure 18 – Cross-section of head-on type PMT [30]

This PMT measures 28 mm in diameter with an effective diameter of 25 mm. The effective diameter of this PMT matches the diameter of the CLYC crystal. The spectral response of this PMT is 300 to 650 nm, peaking at 350 nm. It is also a head-on type PMT with super bialkali (SBA) photocathodes [32]. Other pertinent properties of the Hamamatsu R3998-100-02HA PMT are included in Table 5.

Table 5 – Properties of the Hamamatsu R3998-100-02HA PMT [31]

Property	Value
Dynode Stages	9
[Max. Rating] Anode to Cathode Voltage	1500 V
[Max. Rating] Average Anode Current	0.1 mA
Anode to Cathode Supply Voltage	1000 V
[Cathode] Luminous Sensitivity Min.	100 μA/lm
[Cathode] Luminous Sensitivity Typ.	135 μA/lm
[Cathode] Blue Sensitivity Index (CS 5-58) Typ.	13.5
[Cathode] Radiant Sensitivity Typ.	110 mA/W
[Anode] Luminous Sensitivity Min.	50 A/lm
[Anode] Luminous Sensitivity Typ.	130 A/lm
[Anode] Radiant Sensitivity Typ.	1.1×10^5 A/W
[Anode] Gain Typ.	1.0×10^6
[Time Response] Rise Time Typ.	1.5 ns
[Time Response] Transit Time Typ.	17 ns

3.1.3 Detector Housing

For final measurements, the encapsulated CLYC crystal was optically coupled to a PMT and then inserted into an aluminum detector housing. This detector housing was designed in the SolidWorks computer-aided design software. The designs of the small and large detector housings are shown in Figure 19 and 20. The final products were machined from aluminum in the UNLV Engineering Machine Shop by Mr. Terrance Kell. The exceptionally thin aluminum walls of the detector housing allow for radiation to easily pass through and to interact with the scintillator. The completed assembly of the 1-inch-diameter, 1-inch-height CLYC detector is shown in Figure 21.

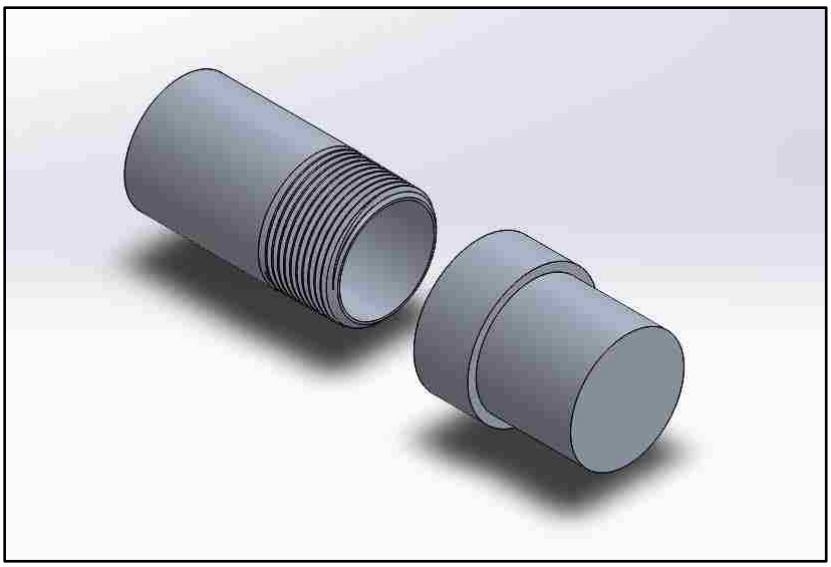

Figure 19 – SolidWorks rendering of 1-inch CLYC detector housing

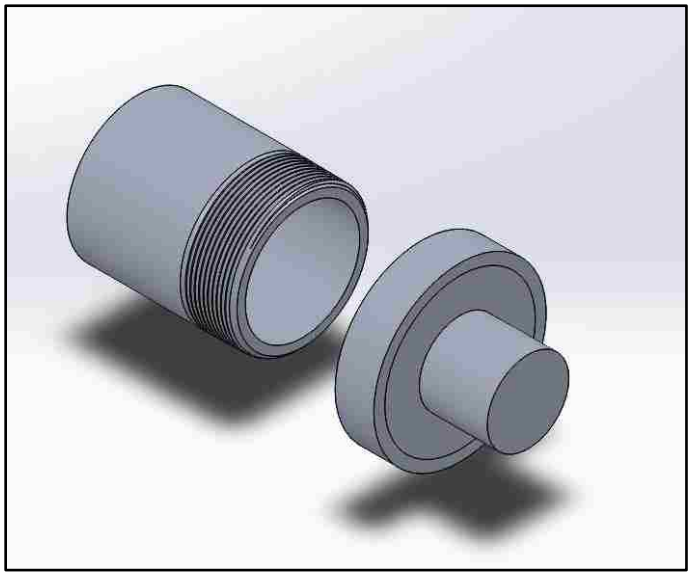

Figure 20 – SolidWorks rendering of 1.5-inch CLYC detector housing

Figure 21 – Completed 1-inch CLYC detector assembly

3.1.4 Digital Data Acquisition and Analysis

The eMorpho digitizer (Bridgeport Instruments) was used for data processing and analysis. It is a single-input digitizer allowing for the collection of data from one scintillating detector [32]. The eMorpho is capable of operating on any device that supports a web browser and it is easily connected to a computer for data analysis via a USB cable. The USB also provides power to the digitizer. It utilizes open source software, a modular firmware structure and an on-board field-programmable gate array (FPGA), which permits the custom development of detection systems. The eMorpho unit is displayed in Figure 22. The eMorpho digitizer collects data from the scintillation pulses produced by the scintillation detector [33]. The current output on the anode of the PMT produced from the scintillation pulses is converted to a voltage signal by the eMorpho. The control parameters including gain, integration time, hold-off time and

trigger threshold can be set using the graphical user interface (GUI) in order to process the incoming signal appropriately. The eMorpho converts the analog voltage signal to a digital waveform by a 12-bit, 100-megahertz waveform-digitizing analog-to-digital converter (ADC). The FPGA processes the resulting waveform, which is then sent to the USB connected computer.

This MCA provides the highest energy resolution and histogram rate for any scintillator [32]. It is capable of performing gated spectroscopy and pulse shape discrimination of different particles. Pile-up rejection is also available. Additional functions of the digitizer include an oscilloscope and list-mode data acquisition capabilities. The extensive functionality, flexible interface and ease of system integration make the eMorpho digitizer ideal for the applications of this study. The eMorpho connected to the assembled CLYC detector was used for the spectroscopy and pulse shape discrimination experiments of this study.

Bridgeport Instruments also developed a data acquisition (DAQ) unit qMorpho. The qMorpho integrates the technology of four 2048-channel eMorpho digitizers into a single unit [34]. It is capable of providing energies, triggers, time stamps, histograms, list mode acquisition and pulse shape analysis. The qMorpho can also be connected to a computer for "on-the-fly" data analysis. However, the qMorpho cannot be powered by the USB cable; it is powered by a standard power cord. The qMorpho DAQ is shown in Figure 22 alongside the eMorpho unit.

The four-channel qMorpho allows for up to four detectors to operate simultaneously. This feature provides the capability of coincidence and gated spectroscopy in addition to pulse shape discrimination of different particles. The

qMorpho features an oscilloscope and list mode data capabilities. The qMorpho was utilized for the directional radiation measurements in this study.

The eMorpho and qMorpho were connected to the pins of the PMT via a high voltage (HV) base. The 2-inch-diameter PMT was connected to a JEDEC 14-pin base (B14-38) for easy integration to the Bridgeport Instruments hvBase-P-B14D08-1. The 1-inch PMT was connected directly to an OEM miniBase from Bridgeport Instruments. These bases provide power to the PMT dynodes and connectivity to the DAQ units [35].

Figure 22 – qMorpho (left) and eMorpho (right) digitizers

3.1.5 Computer Interface

A graphical user interface (GUI) is required in order for users to communicate with the DAQ unit and to analyze the resulting data. The GUI utilized in this study was the IGOR Pro environment by Wavemetrics. It is tailored specifically for experimentation with scientific and engineering data [36]. It possesses the ability to process large amounts of data and perform various engineering analyses including curve fitting, peak analysis,

signal processing and statistics. IGOR Pro also provides high-quality graphs for analysis and presentation. The GUI programming of the aforementioned digitizers was based on IGOR Pro. It is an ideal environment not only because it is the basis for the GUI programming of the eMorpho and qMorpho but, the capabilities of IGOR Pro meet the needs of this study.

3.2 Laboratory Environment

All experiments performed in this study were executed at UNLV in the Nuclear Measurements Laboratory. This laboratory is located in the Thomas Beam Engineering Building (TBE). The laboratory houses a shielded vault containing several radioactive sources. Of these sources, the 2.0-Ci plutonium-beryllium (^{239}PuBe or PuBe) neutron source, 0.8980 μCi ^{137}Cs, 0.9314 μCi ^{60}Co, 0.8294 μCi ^{57}Co and 1.0808 μCi ^{133}Ba gamma-ray sources were utilized in this study.

The PuBe source is a 1-inch-diameter, 2-inch-long sealed source located in a corner of the reinforced concrete shielded vault as shown in Figure 23. This source is contained within a 55-gallon steel drum, 2 ft in diameter and 3 ft in height. The source is surrounded by a thick layer of paraffin for neutron shielding. The PuBe is mounted on to a control rod that rests at approximately 1.33 ft from the bottom of the steel drum. When the control rod is lifted, a neutron beam is formed. When the control rod is lowered, the neutron beam is "closed" off. A circular beam port located approximately 1 ft below the top surface of the steel drum allows for the creation of a neutron beam (when the control rod is in the "up" position) yielding approximately 10^5 neutrons/s. When the source is not being used, a polyethylene cylinder (plug) is placed inside of the port. The PuBe source was used for PSD analysis and directional measurements in this study.

The ^{137}Cs, ^{60}Co, ^{57}Co and ^{133}Ba gamma-ray emitters are shown in Figure 24. These sources were used for calibration of the CLYC detector, measurement of energy spectra, efficiency measurements and directional detection measurements.

Figure 23 – Sealed PuBe neutron source in 55-gal steel drum utilized in this study

Figure 24 – Sealed gamma-ray check sources utilized in this study

3.3 Directional Source Measurements

An array of three CLYC detectors consisting of two 1-inch-diameter by 1-inch-height CLYC crystals and one 1.5-inch-diameter by 1.5-inch-height CLYC crystal was assembled for the purposes of the directional neutron / gamma-ray detection experiments. The first 1-inch CLYC detector, referred to as CLYC #1, is the detector presented in Section 3.1. The second 1-inch CLYC detector, referred to as CLYC #2, and the 1.5-inch CLYC detector, referred to as CLYC #3, were supplied by the NSTec RSL. Utilizing an array of three detectors allows for a decrease in cost and system size without compromising the adequate collection of information so to accurately determine the position of the source being detected. The detector system was set atop a turntable, which provides 360° rotation of the system in the XY-plane. The rotation of the detector system in the XY-plane only will provide data on the longitudinal location of the detected source. In addition to measurements in two dimensions (XY-plane), measurements in all three dimensions (XY- and YZ-plane) will be performed. A latitudinal displacement source holder was used to move the source being detected along the z-axis. Three-dimensional measurements of a radioactive source utilizing this detector system reflect realistic, in-the-field remote sensing conditions for which the longitudinal and latitudinal position of a source of previously unknown location can be determined. The complete detector system, including the detector array, turntable and latitudinal displacement source holder are presented in Figure 25. Data gathered from each detector in the detector system was post-processed using the maximum likelihood estimation algorithm discussed in depth in Section 4.3. This algorithm provides the most-likely direction for which the detected radioactive source is located. The neutron and gamma-ray directional

measurements were also simulated in the Monte Carlo particle transport code MCNP6 for comparison to the experimental results.

This detector system was deployed for directional measurements of the following radioactive sources: ^{137}Cs, ^{60}Co and PuBe. The efficiency of each of the three CLYC detectors was measured. The efficiency was derived from the number of photopeak gamma rays detected and compared to the number of gamma rays emitted from the source. The efficiency for each CLYC detector was calculated utilizing measurements from ^{137}Cs, ^{60}Co, ^{57}Co and ^{133}Ba. Directional gamma-ray measurements were then performed by collecting data from a ^{137}Cs source at different distances from the detector system both in the XY-plane and the YZ-plane.

Figure 25 – CLYC detector system mounted to turntable, adjacent to latitudinal displacement source holder

Directional gamma-ray measurements were also performed for a two-source case in which a ^{137}Cs and a ^{60}Co source were placed in two different positions in proximity to the detector system. This experiment was repeated once more, but with the two gamma-ray sources positioned in the same location. The final directional measurements were performed with the PuBe neutron source. The fast neutrons emitted from this source are thermalized using a polyethylene moderator. Directional measurements were taken at several distances from the PuBe neutron source. The directional measurements of these sources, coupled with comparison to computational results, provide insight into the capabilities of the CLYC detector as a dual neutron / gamma-ray directional detector.

CHAPTER 4

COMPUTATIONAL STUDY

4.1 Modeling of Elpasolite Detector Responses

In addition to the emission of alpha particles upon the capture of thermal neutrons by ^{6}Li, prompt gamma rays are also emitted upon the capture of thermal neutrons by chlorine nuclei contained within the CLYC scintillator. Notable characteristic gamma rays emitted from this interaction are produced at 516 keV, 788 keV, 1165 keV, 1951 keV, 1959 keV, 2864 keV, 5715 keV, 6111 keV, 6619 keV, 7414 keV and 7790 keV [37]. Pertinent information concerning thermal neutron captures can be obtained by studying these gamma rays.

A computational study utilizing the MCNP6 code was used to evaluate the gamma rays produced by thermal neutron captures on the chlorine nuclei of the CLYC scintillator [38]. This study allows for the determination of which aforementioned characteristic gamma-ray peaks are most visible in the measured gamma-ray spectrum.

An F4 tally calculating the flux of gamma rays was used in the MCNP input code to model the spectral distribution for the gamma rays and neutrons within three different simulated scintillators: CLYC, sodium chloride (NaCl) and natural abundance chlorine (Cl). Each simulated scintillator is 1 inch in diameter and 1 inch in height. The simulated CLYC scintillator contains natural abundance chlorine (^{37}Cl 24.23%, ^{35}Cl 75.77%) and 100% enriched ^{6}Li with a density of 3.31 g/cm^{3}. The NaCl scintillator was modeled based on common table salt with a density of 0.003214 g/cm^{3}. The natural abundance chlorine contains 24.23% ^{37}Cl and 75.77% ^{35}Cl with a density of 2.17 g/cm^{3}. An isotropic thermal neutron point source was placed 20 cm from the scintillator face. The collected data

reveals which gamma-ray peaks produced from thermal neutron capture on chlorine nuclei are visible within the gamma-ray spectrum. By comparing the CLYC scintillator to NaCl and natural abundance Cl, one is able to observe the contribution of Cl to the production of these gamma rays.

4.2 Modeling of Directional Neutron / Photon Detection

A detector system consisting of an array of three CLYC detectors was modeled with the Monte Carlo particle transport code MCNP6. The response of the detector system to both an isotropic neutron source and an isotropic gamma-ray source was determined. The detector system was modeled in MCNP6 as presented in Figure 26. This is a simplified model consisting of only three CLYC scintillator crystals each encapsulated in an aluminum housing. Other parts of the detector system have little effect on the radiation interactions within the CLYC crystal. Recall that the array consists of two 1-inch-diameter by 1-inch-height CLYC crystals and one 1.5-inch-diameter by 1.5-inch-height CLYC crystal. In the computational model, all three CLYC crystals are 1-inch-diameter by 1-inch-height. By modeling all three CLYC crystals of the same size, the computational results can more adequately reflect the experimental results for which the 1.5-inch-diameter by 1.5-inch-height CLYC crystal response has been normalized to the response of the 1-inch-diameter by 1-inch-height crystals.

In addition to modeling the three-detector array, an array of four CLYC detectors was modeled for comparison. This comparison illustrates any differences in quality between the three detector array and the four detector array.

MCNP6 runs were performed for both the three and the four detector system and for both a neutron source and a gamma-ray source. These MCNP6 models reflected the

directional detection experimental studies discussed previously and provide a means for comparison. Two MCNP6 input codes are included in Appendix A representing the three CLYC detector array exposed to a neutron source and a gamma-ray source. Two additional MCNP6 input codes are also included in Appendix A representing the four CLYC detector array exposed to a neutron source and a gamma-ray source.

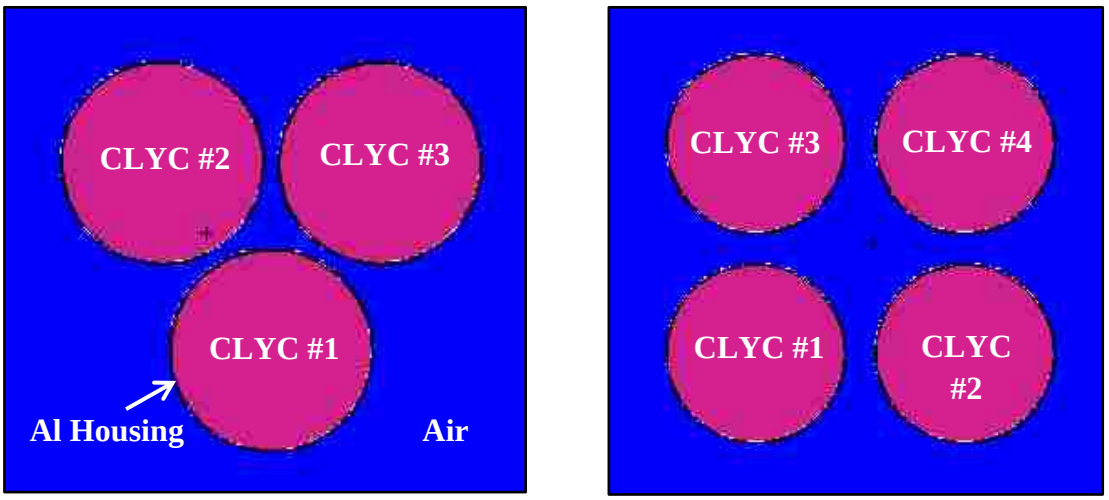

(a) **(b)**

Figure 26 – MCNP6 three-detector and four-detector model

For the neutron source, an isotropic 0.0253 eV thermal neutron source was moved along a path of a circle in increments of 40°, from 0° to 360°, at a distance of 1 m from the origin (0,0,0) for near field measurements and at a distance of 3 m from the origin for far field measurements in the XY-plane. These conditions reflected those used in the experimental study. To calculate the number of thermal neutron captures on ^{6}Li within the CLYC crystal, an F8 tally (which calculates the energy distribution of pulses created in a detector by incident radiation) with an FT8 CAP treatment was used. The FT8 CAP treatment turns the F8 tally into a neutron capture tally, which returns the number of neutron captures on ^{6}Li in the CLYC crystal. The number of neutron captures counted in

each of the detectors as a function of source position provided the directional response of the detector system to the thermal neutron source.

For the gamma-ray source, an isotropic 662 keV gamma-ray source (representative of ^{137}Cs) was also moved along a path of a circle in increments of 40°, from 0° to 360°, at a distance of 10 cm from the origin (0,0,0) for near-field measurements and at a distance of 20 cm from the origin for far-field measurements in the XY-plane and at a height of 0 cm and 10 cm in the YZ-plane. These conditions were reflective of the experimental directional detection study for ^{137}Cs. To calculate the number of gamma rays interacting within the CLYC crystal, an F4 tally (average flux over the crystal) was utilized. The gamma-ray flux, in units of photons/cm^2, counted in each of the detectors as a function of the source position multiplied by the surface area of the detector face and an additional multiplication factor provides the directional response of the detector system to the gamma-ray source.

4.3 Maximum Likelihood Estimation Algorithm

The statistical analysis referred to as maximum likelihood estimation (MLE) provides means to estimate unknown parameters provided a set of data. In the computational and experimental directional detection study, the direction of the radioactive source being measured was known. However, if this directional detection system would be employed in-the-field to find a lost, stolen or smuggled radioactive source or nuclear material, the exact position of the source will most likely not be known. Applying the maximum likelihood estimation algorithm (MLEA) discussed below to 360°-measurements collected by the directional detection system will produce an estimation of the direction for which the source is located. This algorithm was applied to

all of the results from the experimental and computational study of the directional detection system.

Assuming that the counts in each detector of the directional detection system collected over a range of angles from 0° to 360° are normally distributed, the probability density function (PDF) of this normal distribution is as follows:

$$f(N|(\alpha,\sigma^2)) = \frac{1}{\sqrt{2\pi}\sigma} e^{-\frac{(N-\alpha)^2}{2\sigma^2}} \quad \text{(Equation 6)}$$

Given the above PDF, the likelihood function and log-likelihood function are the following, respectively:

$$\boldsymbol{\varphi(\alpha,\sigma^2)} = \prod_{i=1}^{n} \frac{1}{\sqrt{2\pi}\sigma} e^{-\frac{(N_i-\alpha)^2}{2\sigma^2}} \quad \text{(Equation 7)}$$

$$\log \varphi(\alpha,\sigma^2) = \sum_{i=1}^{n} \left(\log \frac{1}{\sqrt{2\pi}} - \log\sigma - \frac{(N_i-\alpha)^2}{2\sigma^2} \right) \quad \text{(Equation 8)}$$

$$= n \log \frac{1}{\sqrt{2\pi}} - n \log \sigma - \frac{1}{2\sigma^2} \sum_{i=1}^{n} (N_i - \alpha)^2$$

$$\alpha = \frac{I_0}{R_i^2} \quad \text{(Equation 9)}$$

$$R_i^2 = x_i^2 + y_i^2 \quad \text{(Equation 10)}$$

where σ is the uncertainty in the measurements, N_i is the counts detected in a single detector at the *i*-th angle (0° to 360°), I_0 is the estimated source intensity, R_i is the estimated distance between the radioactive source and the center of the corresponding detector and x_i and y_i are the estimated coordinates indicative of the direction or angle for

which the radioactive source may be located. The angle corresponding to the maximum of the log-likelihood function is the maximum likelihood estimate for the direction or angle of the radioactive source. The maximum statistical error in the MLEA estimates was 17.5% for the computational study and 0.06% for the experimental study.

CHAPTER 5

RESULTS AND DISCUSSION

5.1 Neutron and Photon Measurements

5.1.1 Photon Measurements

The CLYC detector connected to the eMorpho digitizer / MCA was utilized to measure the gamma-ray spectra of ^{137}Cs and ^{60}Co gamma-ray sources. The CLYC detector was first calibrated to yield the following results utilizing the following parameters: integration time of 4.6 μs, time of return to baseline of 4.9 μs, a coarse gain of 430 Ω and a fine gain of 7065.

The gamma-ray energy spectrum of ^{137}Cs is shown in Figure 27. A Gauss fit of the ^{137}Cs characteristic gamma-ray peak at 662 keV (shown in blue) yields a FWHM / energy resolution of 4.9% and approximately 1496 gamma-ray counts. The gamma-ray spectrum produced by the CLYC detector by the ^{60}Co source is provided in Figure 28 and 29. Figure 28 illustrates the Gauss fit of the first characteristic gamma-ray energy peak of 1173 keV. This fit yields a FWHM / energy resolution of 3.86% and gamma-ray count of 816. Figure 29 shows the Gauss fit for the characteristic gamma-ray energy peak of 1332 keV with a FWHM / energy resolution of 3.6% and gamma-ray count of 812.

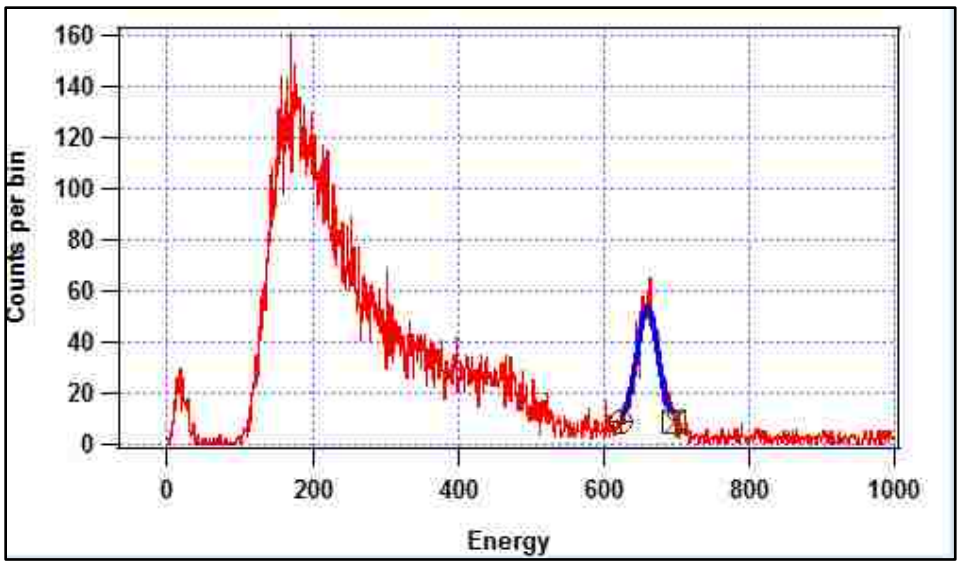

Figure 27 – CLYC measurements of ^{137}Cs photon spectrum

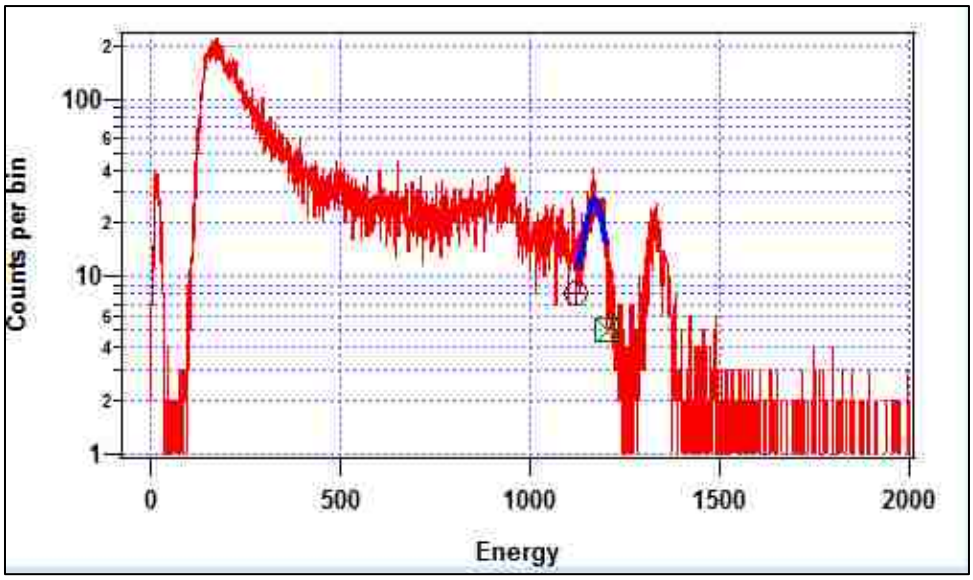

Figure 28 – CLYC measurements of ^{60}Co photon spectrum, Gauss fit at 1173 keV

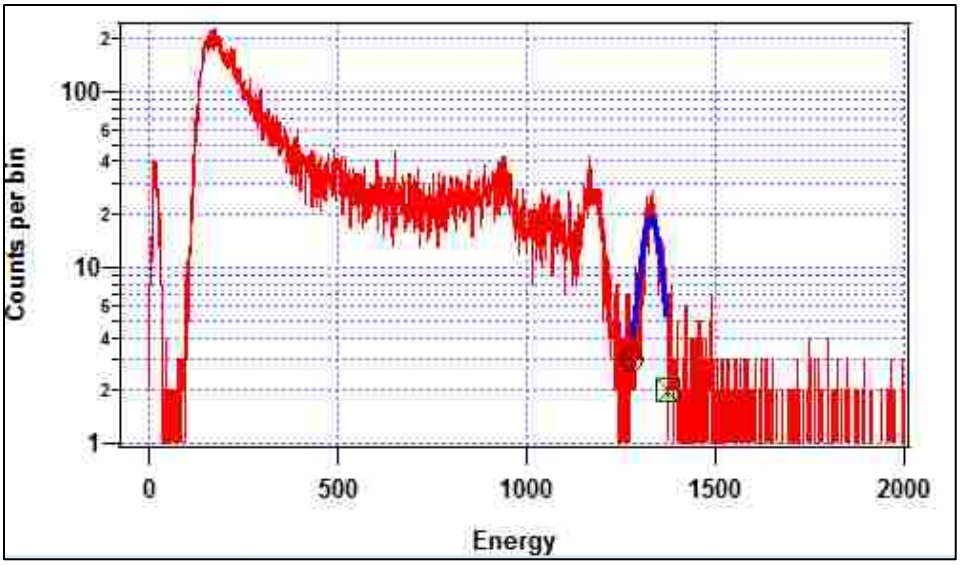

Figure 29 – CLYC measurements of ^{60}Co photon spectrum, Gauss fit at 1332 keV

5.1.2 Neutron Measurements

The CLYC detector coupled to the eMorpho digitizer was utilized to perform PSD measurements using the PuBe source. The detected neutrons and gamma rays each create different signal waveforms. Gamma rays possess a signal waveform with a faster decay rate than those produced by neutrons. Figure 30 demonstrates this difference between the collected neutron and gamma-ray waveforms and how PSD was performed. The partial integration time (PIT) and the integration time (IT) were used to evaluate the front and the tale areas of the pulse. The ratio of the tale and front areas results in the PID value. This PID value was used to separate neutron and gamma-ray signals. The eMorpho is capable of performing such PSD analysis while measurements are being taken. The information gathered during the PSD analysis was stored as list mode data for further analysis post-measurement.

Figure 31 reveals the results of the CLYC detector PSD measurements of the PuBe source. To quantify how well PSD was performed, a figure of merit (FOM) was

calculated using Equation 3 and the parameters presented in Figure 31 (b) for the separation (*T*) and the FWHM for the photon peak and the thermal neutron peak. A FOM of 2.3 was achieved in this experiment. Particles are considered acceptably separated with a FOM ≥ 1.5. It can be clearly observed that the detected neutrons and gamma-rays were successfully detected and separated. The small, circular "cloud" of dots on the right side of Figure 31 (a) is representative of the detected neutrons. The elongated line of dots below the neutron traces is representative of the detected gamma rays.

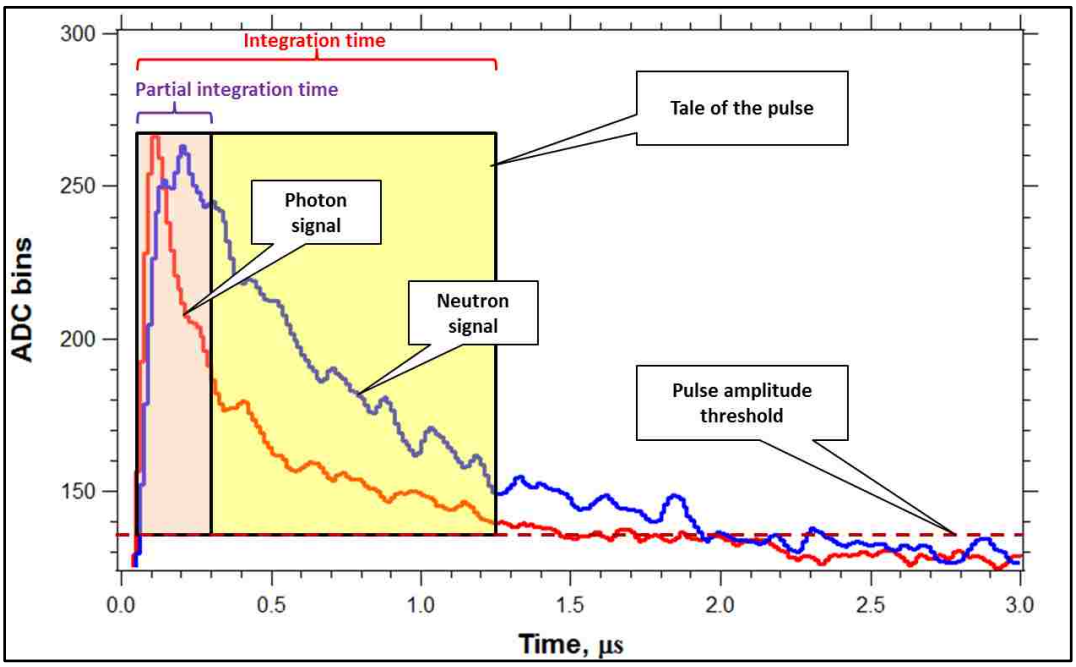

Figure 30 – Pulse shape discrimination scheme

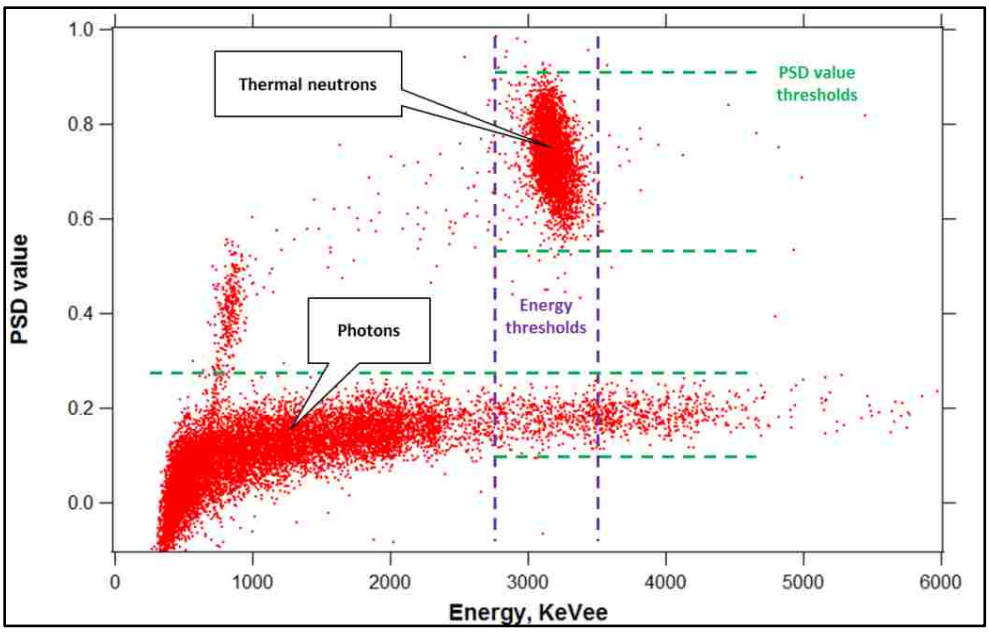

(a)

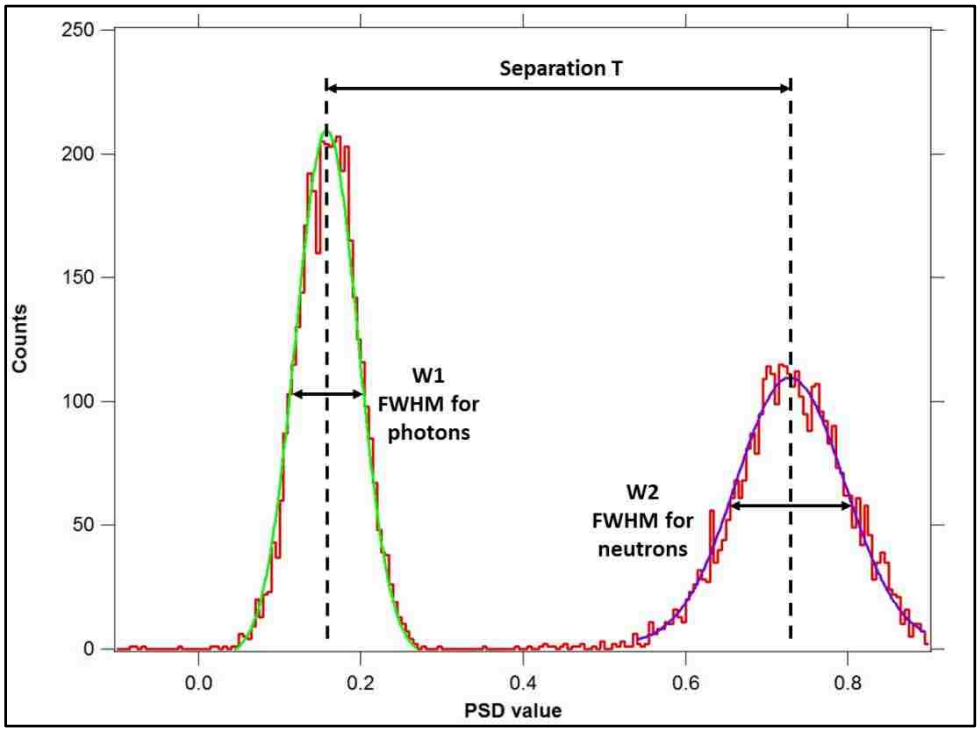

(b)

Figure 31 – CLYC detector PSD measurements of PuBe source

5.2 Monte Carlo Modeling Results

5.2.1 Elpasolite Detector Responses

The thermal neutron-induced gamma-ray spectra resultant of CLYC, NaCl and natural abundance Cl scintillators mentioned in Section 4.1 are provided in Figure 32, 33 and 34, respectively. Each figure presents the flux of gamma rays averaged within the volume of the selected scintillator versus gamma-ray energy in units of MeV. The eleven gamma-ray peaks (516 keV, 788 keV, 1165 keV, 1951 keV, 1959 keV, 2864 keV, 5715 keV, 6111 keV, 6619 keV, 7414 keV and 7790 keV) created due to thermal neutron capture on Cl nuclei are readily visible with the natural abundance Cl scintillator in Figure 34. These peaks are also visible in the NaCl and the CLYC scintillators (Figure 33 and 32, respectively), but with less intensity / resolution. In addition to the aforementioned peaks, the 477 keV gamma-ray peak due to the ^{7}Li (n,n'γ) reaction can be observed in the gamma-ray spectrum produced by the CLYC scintillator containing ^{7}Li. The ability to observe the gamma-ray peaks produced by thermal neutron capture on Cl in the CLYC scintillator indicates that they should be taken into account in spectrometry in mixed radiation fields (neutron and photons).

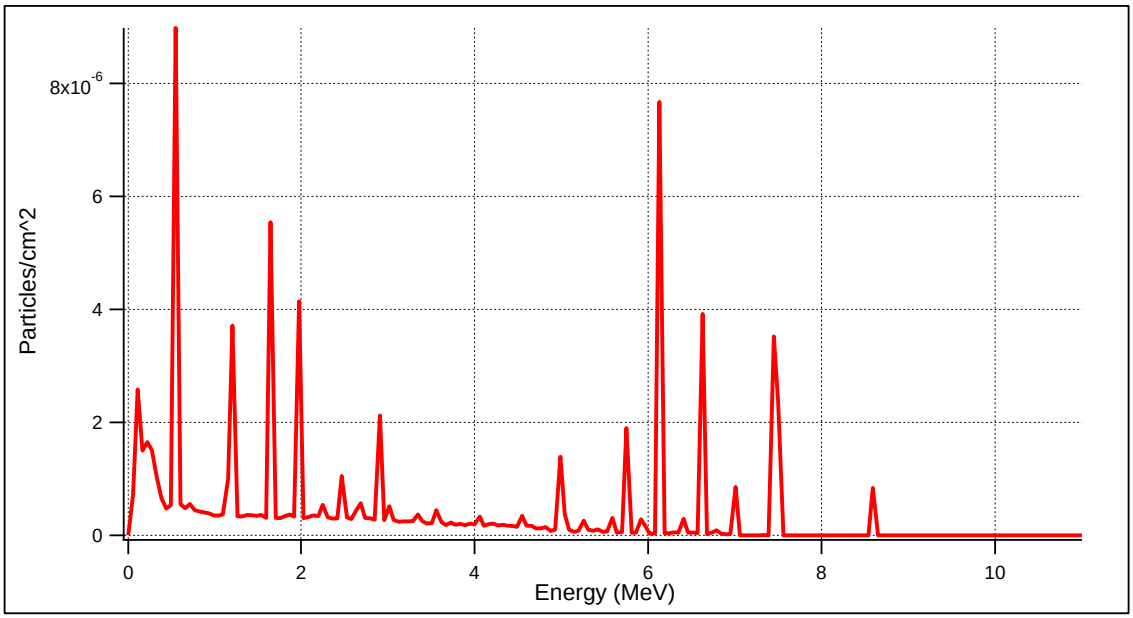

Figure 32 – Thermal neutron induced gamma rays in the 1"×1" CLYC

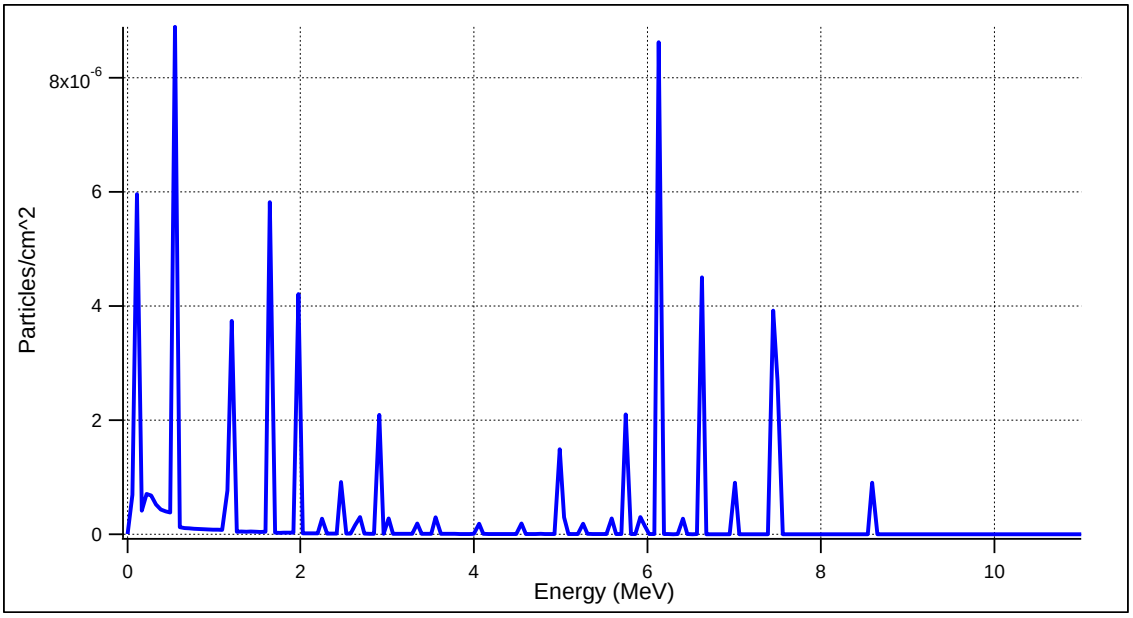

Figure 33 – Thermal neutron induced gamma rays in the 1"×1" NaCl scintillator

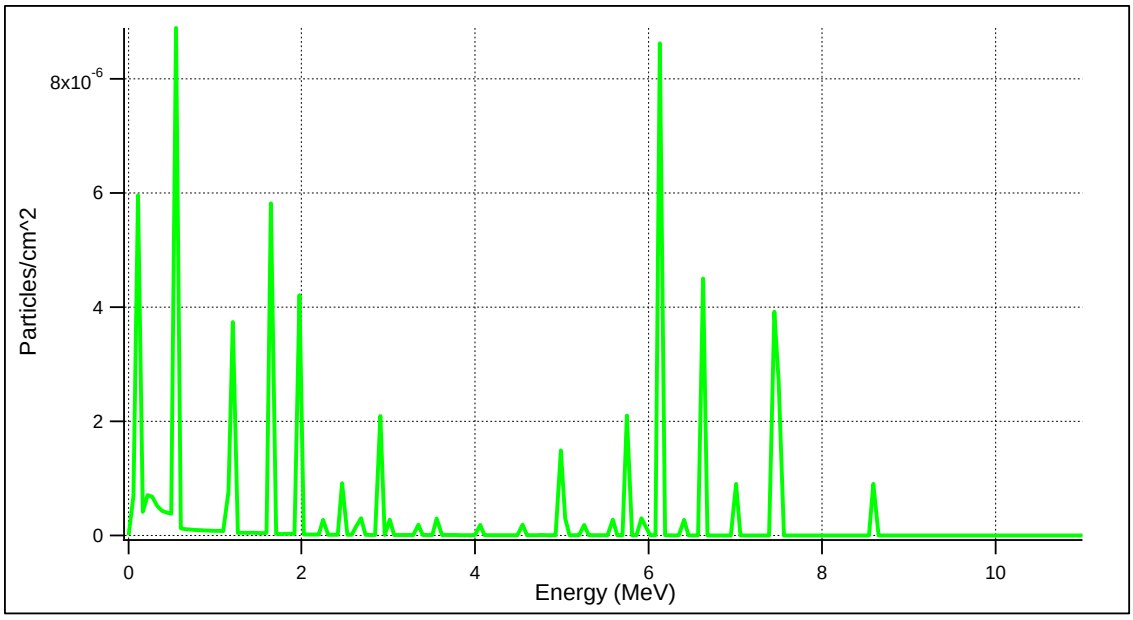

Figure 34 – Thermal neutron induced gamma rays in the 1"×1" natural chlorine scintillator

5.2.2 Modeling of Directional Neutron / Photon Detection

The MCNP6 modeling results are prognostic of the experimental results to come. The input models of the directional detection system consisting of the three CLYC detector array, as previously described in Section 4.2, provide advantageous information on how the experimental directional detection system responds to a radioactive source in both the longitudinal and latitudinal directions. The models of the four CLYC detector array serve as a comparison to the three CLYC detector array in terms of quality of array response. It can be observed from Figures 35 – 42 and the MLEA estimates provided in Table 6 that the response of both detection systems to neutrons and gamma-rays is similar. The maximum statistical error achieved in the gamma-ray computational study for CLYC #1 was 8.05%, for CLYC #2 8.18% and for CLYC #3 was 8.56%. The maximum statistical error achieved in the thermal neutron computational study for CLYC #1 was 13.6%, for

CLYC #2 17.5% and for CLYC #3 was 14.7%. The quality and magnitude of the response from the three CLYC detector array is comparable if not equal to that of the four CLYC detector array. From this, it can be concluded that a four CLYC detector array is not required to accurately estimate the source direction. A three CLYC detector array will cost less, weigh less and be more compact than a four detector array without decreasing the quality of the directional data and direction estimates.

For near-field measurements, the response of the detectors is higher in magnitude and quality. Measurements in the far-field position are lower in magnitude and appear distorted. This characteristic is due to the fact the intensity of a source decreases with respect to the inverse of the distance from the center of the detector system to the source squared. It can also be observed that as a detector moves closer to a source, the magnitude of the response of that detector increases. Similarly, as a detector moves farther away from the source, the magnitude of the detector's response to the source decreases. This characteristic is apparent when the detectors are rotated 360° in the XY-plane and the YZ-plane. The MLEA estimates for all of the computational models are provided in Table 6. There is no percent error in these estimates, providing the correct estimation for each source direction.

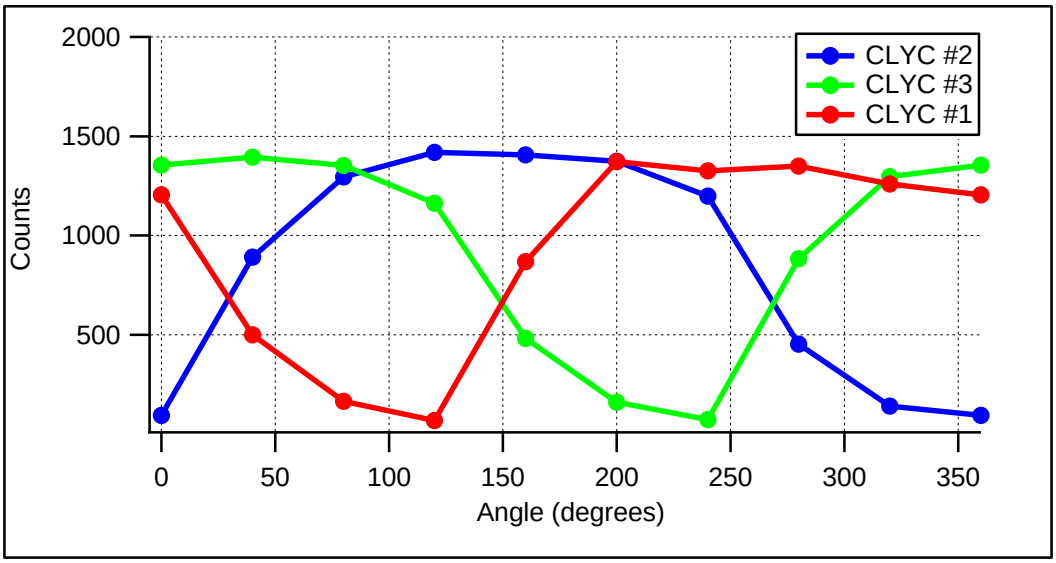

Figure 35 – Three CLYC detector array exposed to thermal neutron source, R=1 m, z=0 m

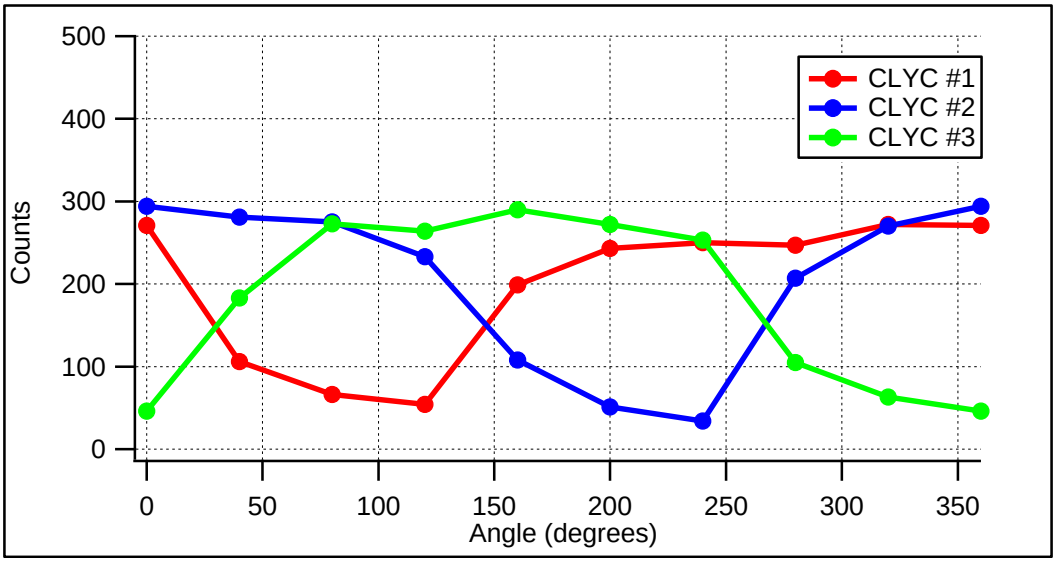

Figure 36 – Three CLYC detector array exposed to thermal neutron source, R=3 m, z=0 m

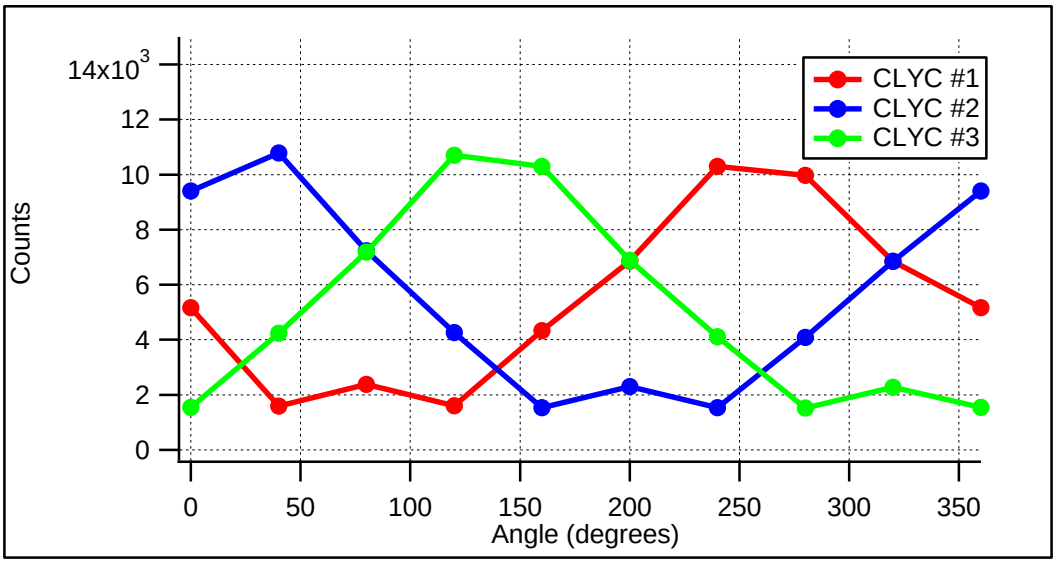

Figure 37 – Three CLYC detector array exposed to ^{137}Cs gamma-ray source, R=10 cm, z=0 cm

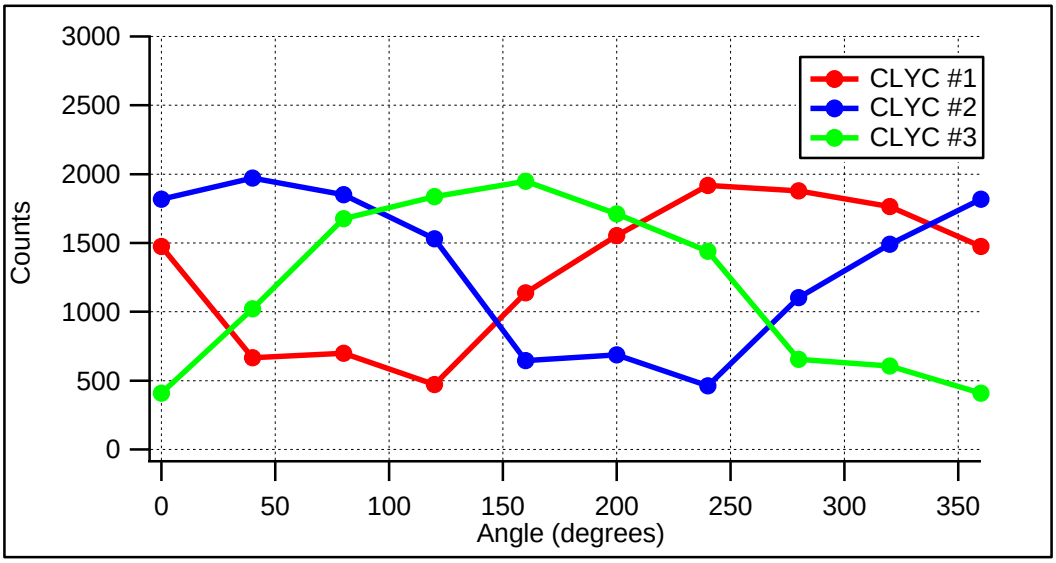

Figure 38 – Three CLYC detector array exposed to ^{137}Cs gamma-ray source, R=20 cm, z=0 cm

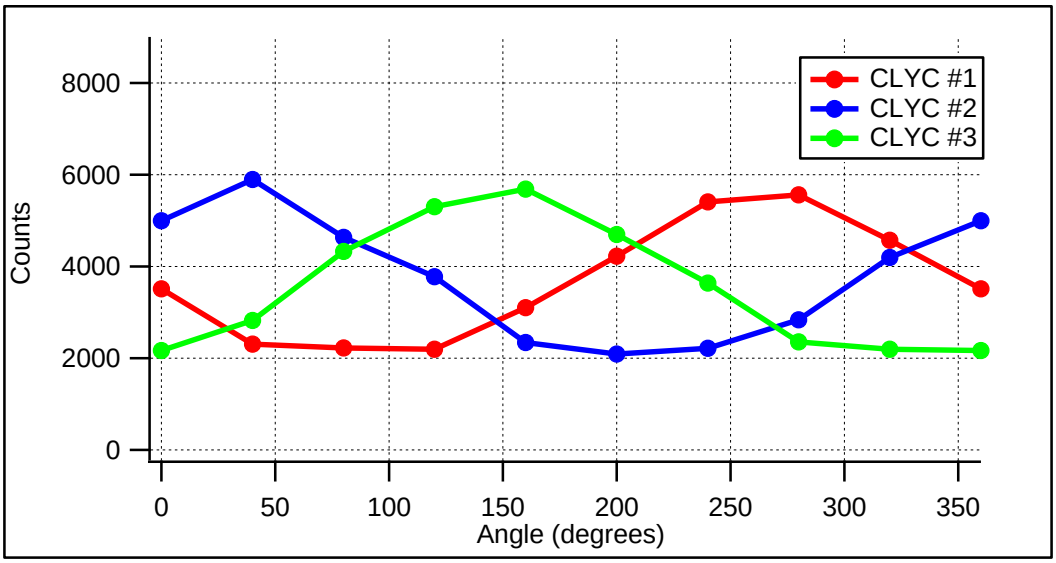

Figure 39 – Three CLYC detector array exposed to ^{137}Cs gamma-ray source, R=10 cm, z=10 cm

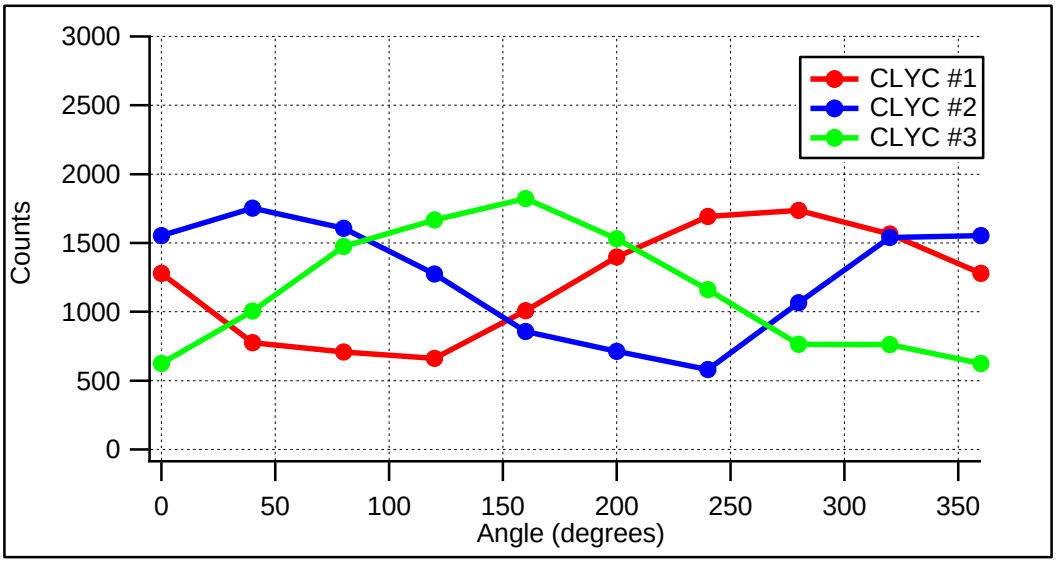

Figure 40 – Three CLYC detector array exposed to ^{137}Cs gamma-ray source, R=20 cm, z=10 cm

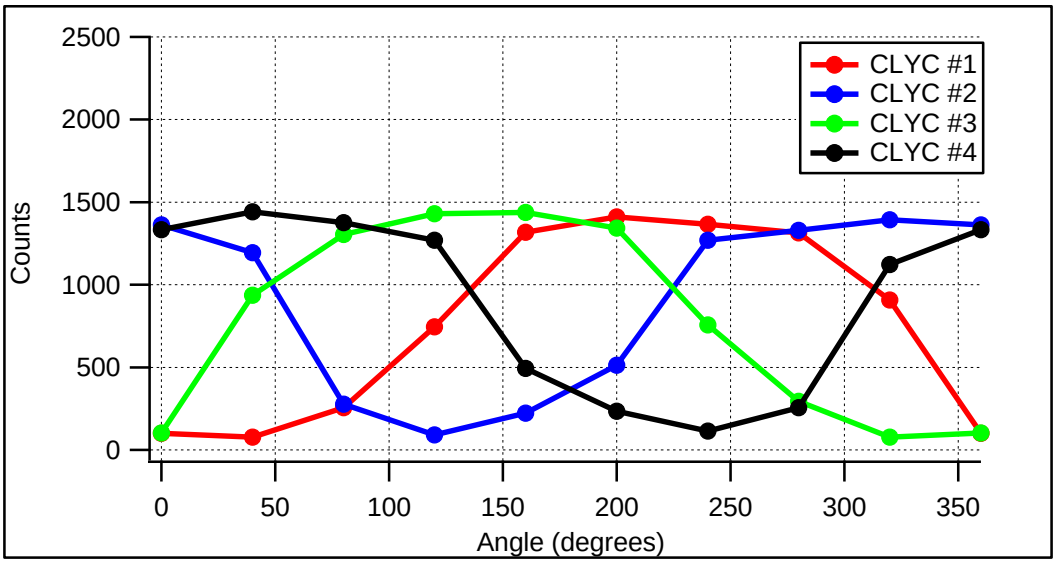

Figure 41 – Four CLYC detector array exposed to thermal neutron source, R=1 m, z=0 m

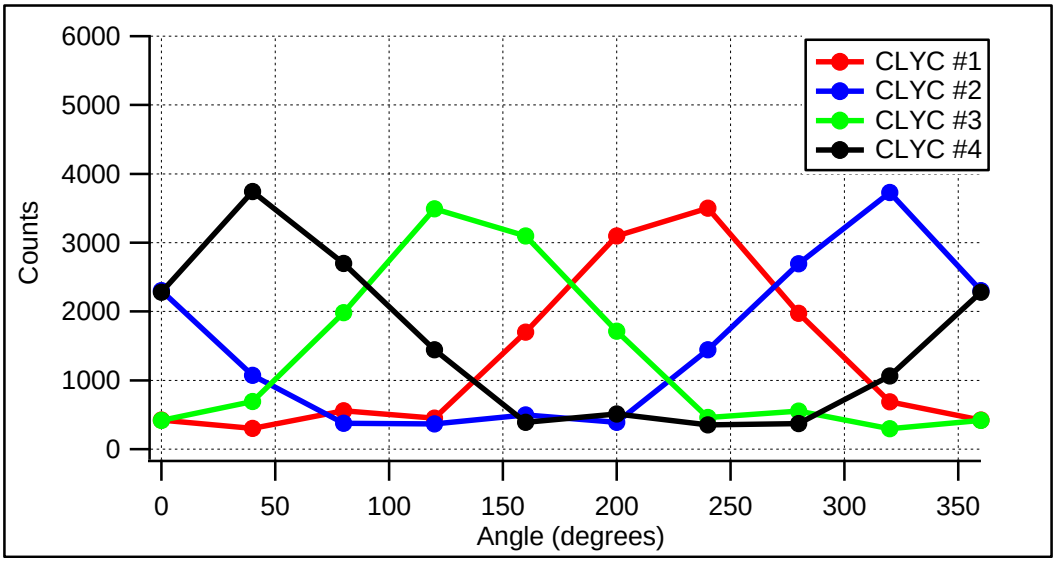

Figure 42 – Four CLYC detector array exposed to gamma-ray source, R=10 cm, z=0 cm

Table 6 - Computational directional measurements MLEA source direction estimates

Actual Source Position	Actual Source Direction	MLEA Source Direction	Error (%)
3-detector, ^{137}Cs: R=10 cm, z=0 cm	40°	40°	0
3-detector, ^{137}Cs: R=20 cm, z=0 cm	40°	40°	0
3-detector, ^{137}Cs: R=10 cm, z=10 cm	40°	40°	0
3-detector, ^{137}Cs: R=20 cm, z=10 cm	40°	40°	0
3-detector, thermal neutrons: R=1 m, z=0 m	40°	40°	0
3-detector, thermal neutrons: R=3 m, z=0 m	40°	40°	0
4-detector, ^{137}Cs: R=10 cm, z=0 cm	40°	40°	0
4-detector, thermal neutrons: R=1 m, z=0 m	40°	40°	0

5.3 Directional Measurements using Three-Sensor System

5.3.1 Detector Efficiency

The detector efficiency quantifies the level of performance characteristic of a radiation detector. It is a physical measure of the number of particles detected by the detector compared to the number of particles emitted from the source. In calculating the efficiency of all three CLYC detectors employed in this study, the number of photo peak gamma rays detected is compared to the total number of gamma rays emitted from the

source. This is referred to as the intrinsic peak efficiency. This efficiency was calculated using data from ^{137}Cs, ^{60}Co, ^{57}Co and ^{133}Ba implemented into the following equations:

$$\varepsilon_{abs} = \frac{\#\ of\ particles\ detected}{\#\ of\ particles\ incident\ on\ detector} \quad \text{(Equation 11)}$$

$$\varepsilon_{int,peak} = \frac{\#\ of\ particles\ detected}{\#\ of\ particles\ emitted} = \varepsilon_{abs}\frac{4\pi}{\Omega} \quad \text{(Equation 12)}$$

$$\Omega = Solid\ Angle = \frac{A}{d^2} \quad \text{(Equation 13)}$$

where *A* is the area of the detector face and *d* is the distance from the radioactive source to the detector face.

Four gamma-ray sources are utilized in determining the intrinsic peak efficiency: ^{133}Ba (356 keV), ^{57}Co (122 keV), ^{137}Cs (662 keV) and ^{60}Co (1173 keV and 1332 keV). This assortment of sources is selected to cover a range of gamma-ray energies. It is characteristic for detector efficiency, including intrinsic peak efficiency, to decrease as gamma-ray energy increases. This characteristic was observed in measuring the intrinsic peak efficiency of the three CLYC detectors utilized in the directional detection study. Figure 43 below depicts this behavior.

Table 7 provides the intrinsic peak efficiency values for each of the three CLYC detectors at a distance of 1 cm from each of the sources. An ideal detector would detect all particles emitted from a radioactive source and thus have an efficiency of 100%. Although the intrinsic peak efficiencies of each of the three CLYC detectors studied are not ideal, these efficiencies are equal to if not better than the "gold standard" NaI(Tl) detector [39]. The largest statistical error found from these measurements for CLYC #1

was 0.027%, for CLYC #2 was 0.026% and for CLYC #3 was 0.030%. The differences in efficiency are a resultant of differences in scintillator crystal size, incident gamma-ray energy and shielding effects of the scintillator / housing among other less influential parameters.

In addition to the calculation of the intrinsic gamma-ray peak efficiency, the intrinsic thermal neutron peak efficiency was calculated for each of the three CLYC detectors at a distance of 50 cm from an isotropic, mono-energetic thermal neutron source modeled in MCNP6. The resulting efficiencies are included in Table 7. These calculated thermal neutron peak efficiencies were comparable to that found by RMD, Inc. in partnership with the University of Michigan [40]. The thermal neutron intrinsic peak efficiency achieved in that study was 10% utilizing a 2-cm-diameter, 2-cm-height CLYC scintillator.

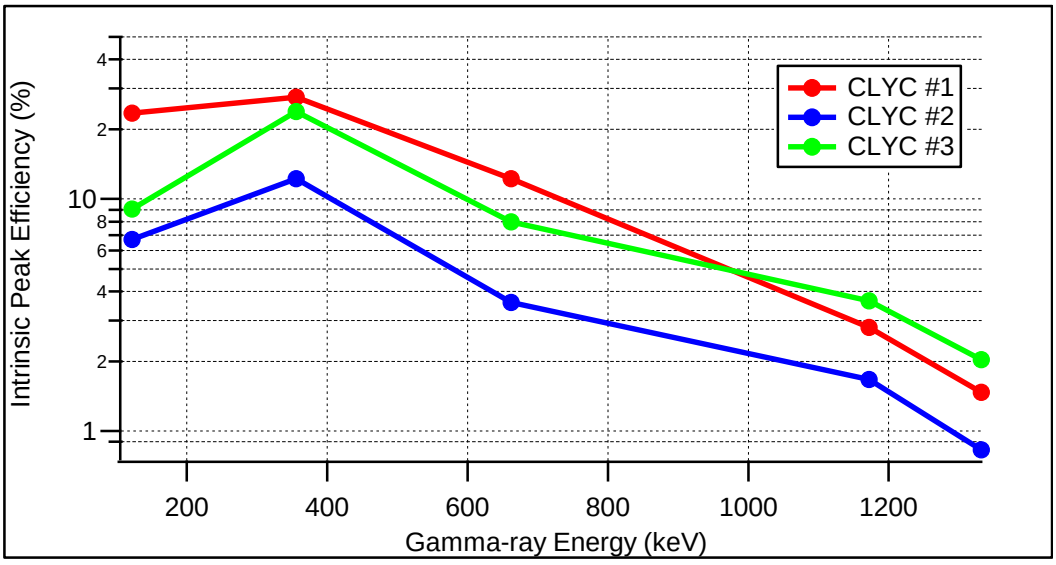

Figure 43 – Intrinsic peak efficiency versus gamma-ray energy

Table 7 – Intrinsic peak efficiencies for CLYC detectors

Detector #	^{57}Co (122 keV) Efficiency	^{133}Ba (356 keV) Efficiency	^{137}Cs (662 keV) Efficiency	^{60}Co (1.17 MeV) Efficiency	^{60}Co (1.33 MeV) Efficiency	Thermal Neutron Source (3.0 MeV (GEE))
CLYC #1	23.4%	27.5%	12.2%	2.80%	1.47%	11.8%
CLYC #2	6.70%	12.2%	3.58%	1.67%	0.83%	11.8%
CLYC #3	9.04%	23.8%	7.97%	3.64%	2.03%	12.6%

5.3.2 Gamma-Ray Measurements

The three-detector array was deployed first for directional gamma-ray measurements. It is the goal of this study to determine the direction for which the gamma-ray source is located. The three CLYC detectors were mounted to the turntable to provide 360°-motion. A ^{137}Cs gamma-ray source was placed on the latitudinal displacement source holder. This experimental configuration is presented in Figure 45 and 46. The source was first placed in-plane with the CLYC crystals and measured at a longitudinal distance of 10 cm and then at a distance of 20 cm from the center of the detectors. The ^{137}Cs source was then moved 10 cm in the vertical direction and measurements were repeated at a longitudinal distance of 10 cm and then 20 cm. Measurements were collected at the following angles: 0°, 40°, 80°, 120°, 160°, 200°, 240°, 280° and 320°.

The results of these measurements are presented graphically in Figure 48, 49, 50 and 51. The maximum statistical error achieved in this measurement for CLYC #1 was

0.03%, for CLYC #2 was 0.02% and for CLYC #3 was 0.02%. These results, accompanied by the MLEA source direction estimates, are tabulated in Table 8. No difference exists between the estimated source direction and the actual direction for measurements collected at R=20 cm, z=0 cm and R=20 cm, z=10 cm. However, there does exist a small discrepancy for measurements collected at R=10 cm, z=0 cm and R=10 cm, z=10 cm. It is hypothesized that these discrepancies in source direction can be eliminated by utilizing a directional detection system of identical CLYC detectors of the same size and quality, identical photomultiplier tubes and identical aluminum housings. This hypothesis is confirmed by the zero percent error achieved in the MLEA estimates of the computational study produced by a homogeneous directional detection system.

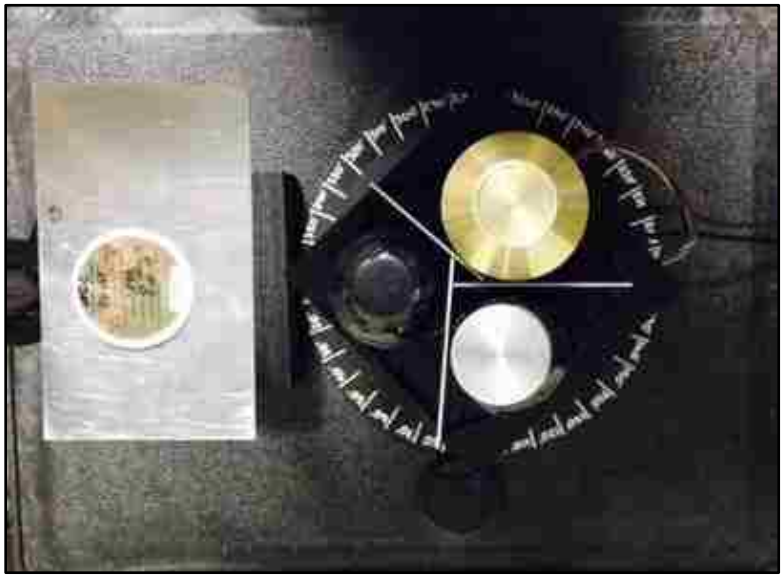

Figure 44 – ^{137}Cs gamma-ray directional measurements experimental setup, top view

Figure 45 – ^{137}Cs gamma-ray directional measurements experimental setup, angled view

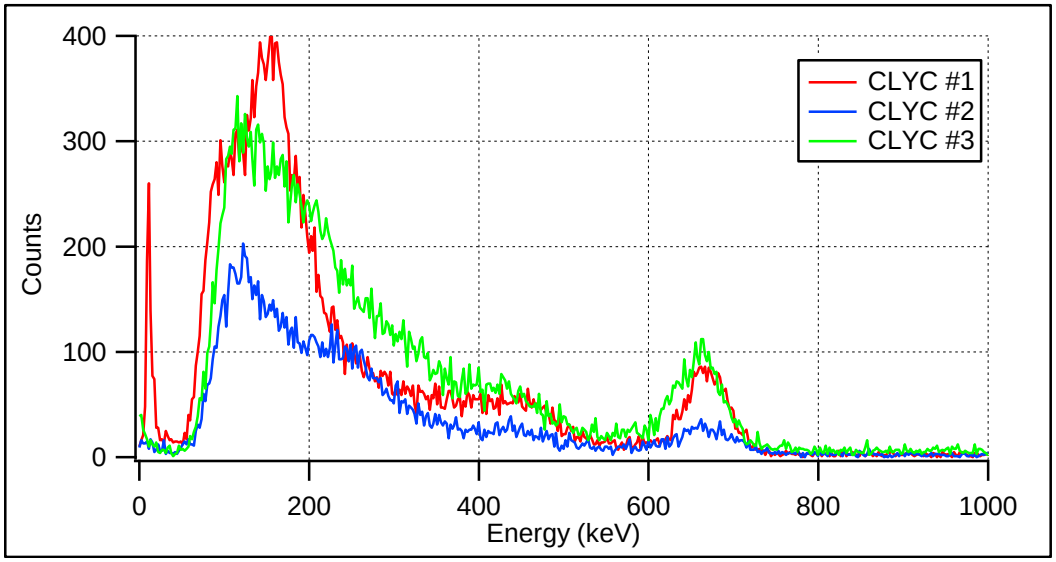

Figure 46 – ^{137}Cs gamma-ray spectra at 0°

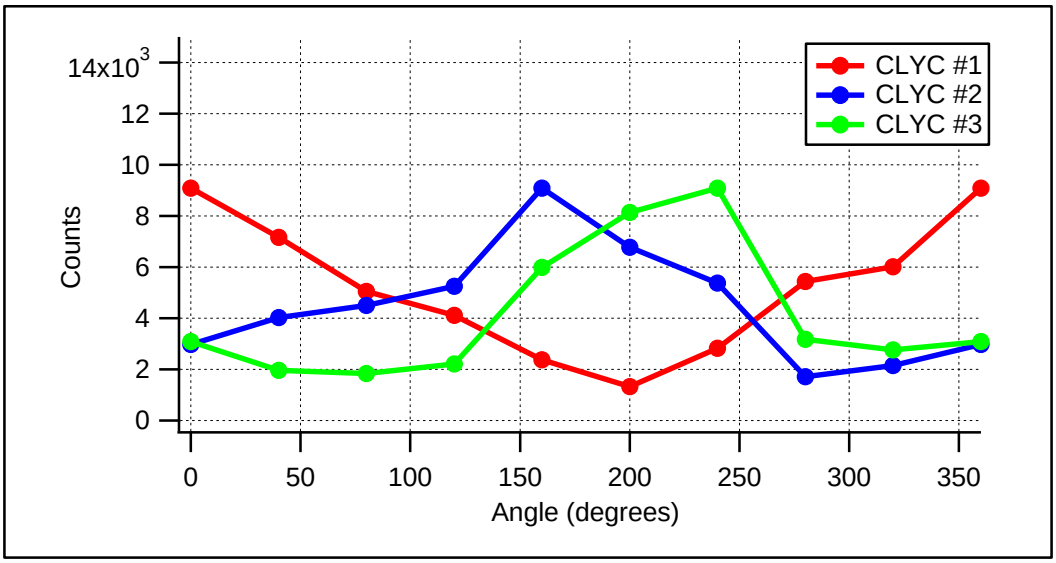

Figure 47 – ^{137}Cs gamma-ray directional measurements results, R=10 cm, z=0 cm

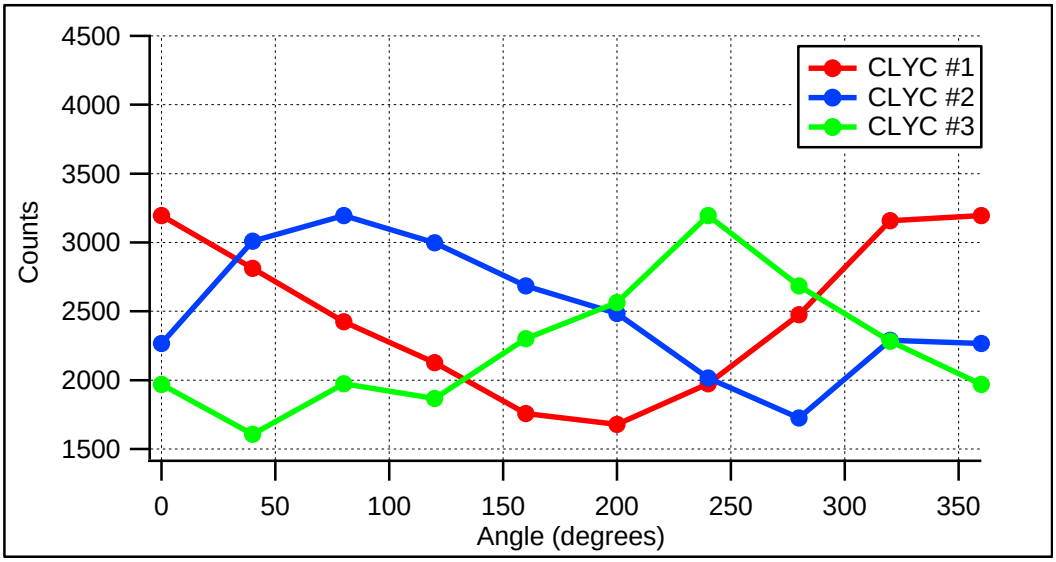

Figure 48 – ^{137}Cs gamma-ray directional measurements results, R=20 cm, z=0 cm

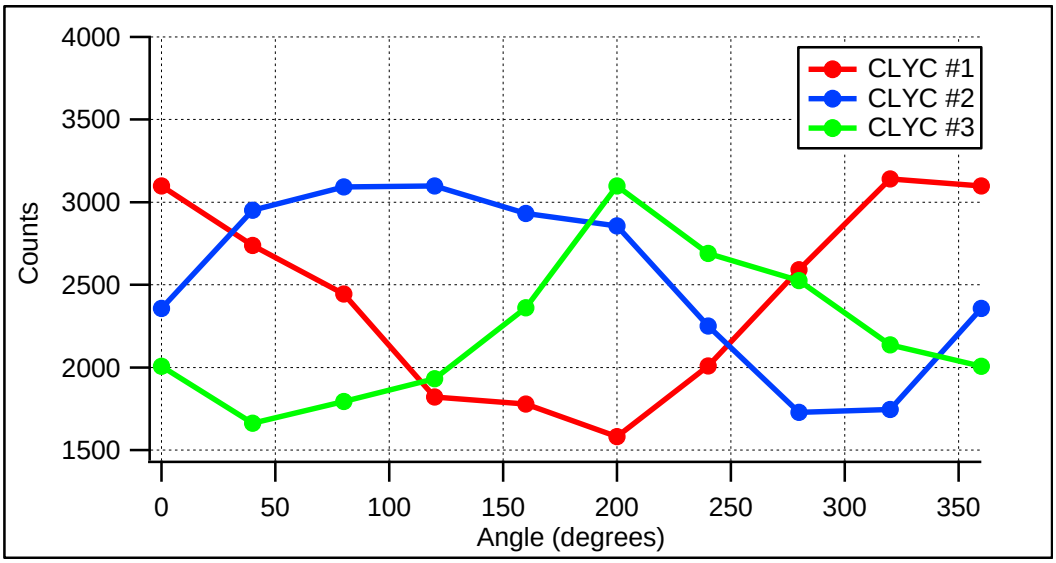

Figure 49 – ^{137}Cs gamma-ray directional measurements results, R=10 cm, z=10 cm

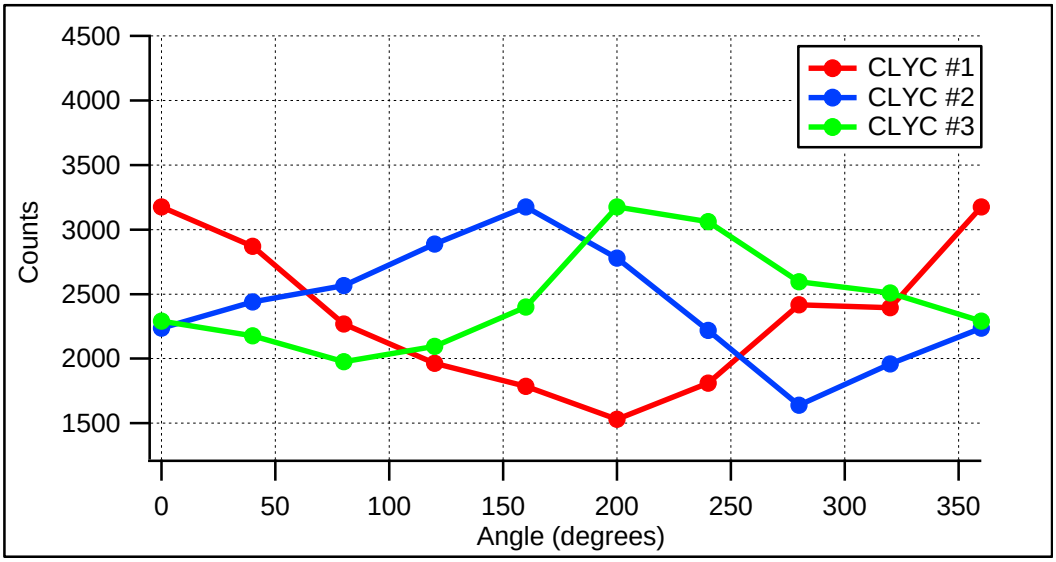

Figure 50 – ^{137}Cs gamma-ray directional measurements results, R=20 cm, z=10 cm

Table 8 – ^{137}Cs gamma-ray directional measurements MLEA source direction estimates

Actual Source Position	Actual Source Direction	MLEA Source Direction	Error (%)
R=10 cm, z=0 cm	0°/360°	13.33°	11.1
R=20 cm, z=0 cm	0°/360°	0°/360°	0
R=10 cm, z=10 cm	0°/360°	333.33°	7.4
R=20 cm, z=10 cm	0°/360°	0°/360°	0

The next set of directional measurements is the two source measurements. A ^{137}Cs and a ^{60}Co gamma-ray source were placed in different positions in proximity to the detector system. It is the goal of this study to locate the direction for which both gamma-ray sources are located. The ^{137}Cs source was placed at the 240° marker of the detection system turntable at a height of -20 cm. The ^{60}Co source was placed in-plane with the CLYC crystals at the 0° marker of the detection system turntable. The experimental setup described is depicted in Figure 51. Measurements are collected at the following angles: 0°, 40°, 80°, 120°, 160°, 200°, 240°, 280° and 320°.

The results of these measurements are presented graphically in Figure 53, 54 and 55. The maximum statistical error achieved in this measurement for CLYC #1 was 0.055%, for CLYC #2 was 0.056% and for CLYC #3 was 0.048%. These results, accompanied by the MLE algorithm source direction estimates are tabulated in Table 9. No discrepancies were found in the estimated direction of either the ^{137}Cs or the ^{60}Co

gamma-ray source; the MLE algorithm estimate for the source directions matched exactly the physical directions of the sources.

Figure 51 – Experimental setup for two source directional measurements

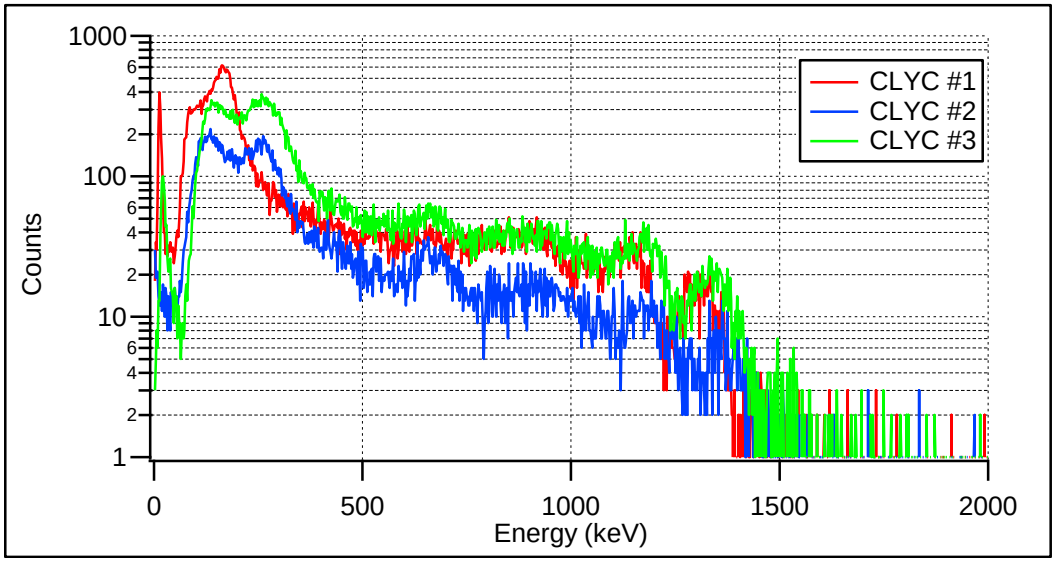

Figure 52 – Two source gamma-ray spectra at 0°

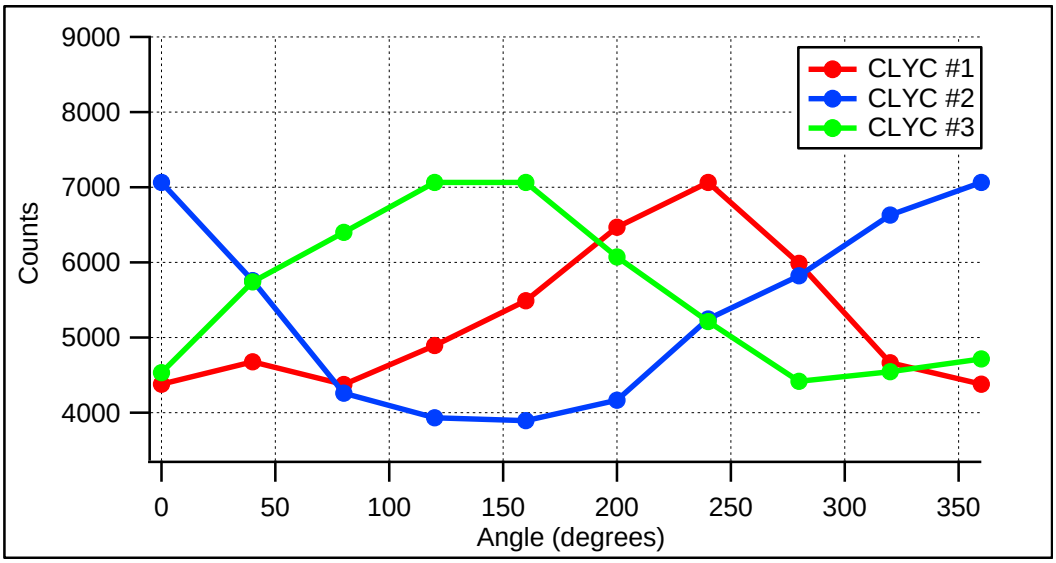

Figure 53 – ^{137}Cs two source directional measurements results

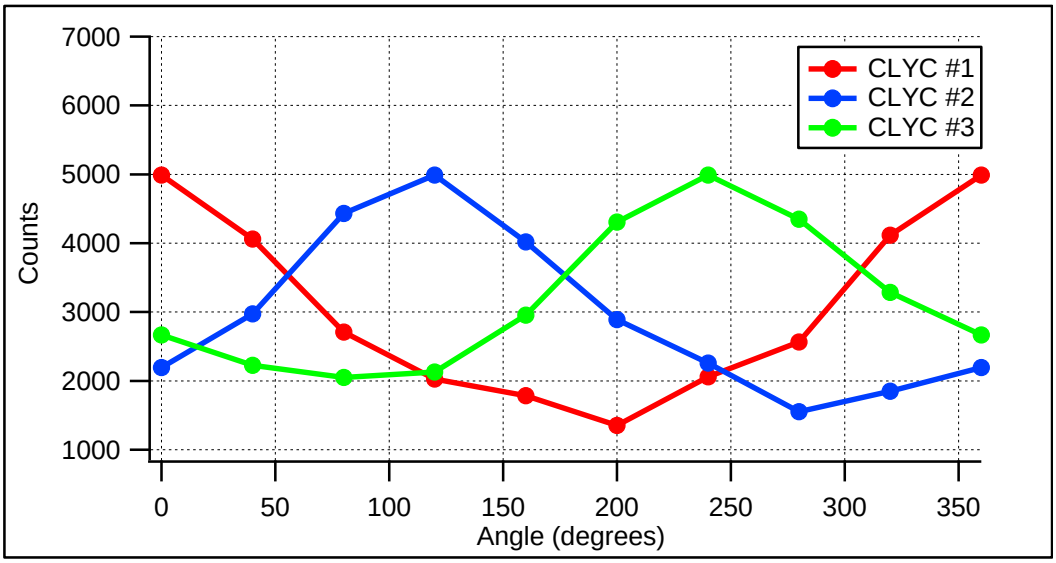

Figure 54 – ^{60}Co (1.17 MeV) two source directional measurements results

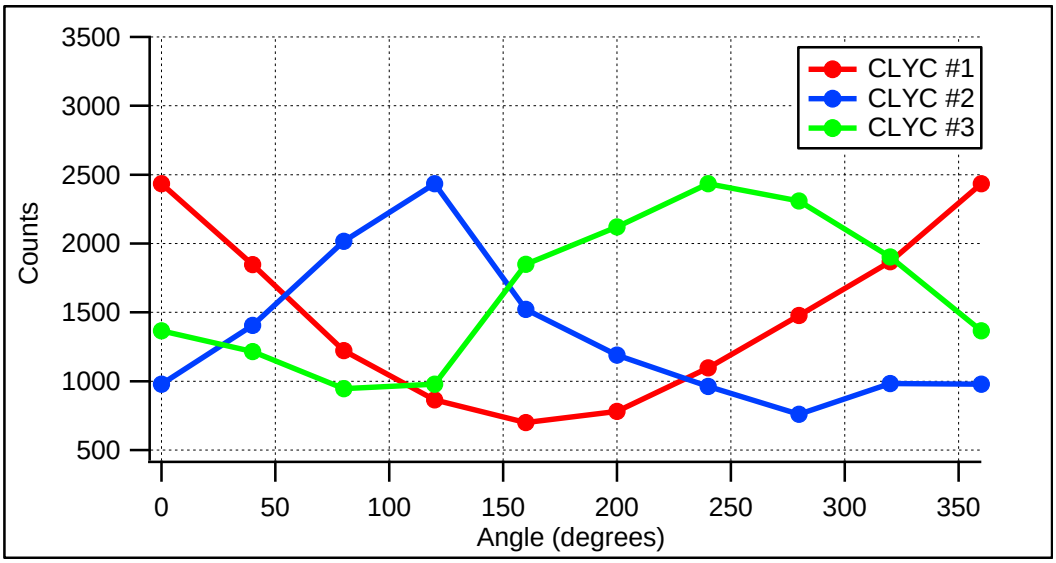

Figure 55 – ^{60}Co (1.33 MeV) two source directional measurements results

Table 9 – Two source MLEA source direction estimates

Actual Source Position	Actual Source Direction	MLEA Source Direction	Error (%)
^{60}Co: R=10 cm, z=0 cm	0°/360°	0°/360°	0
^{137}Cs: R=10 cm, z=-20 cm	240°	240°	0

The ^{137}Cs source was then moved on top of the ^{60}Co source located at R=10 cm and z=0 cm to evaluate how the directional detection system would respond to two co-located gamma-ray sources. It was hypothesized that the directional detection system would be able to detect both the ^{137}Cs and ^{60}Co source and indeed it was able to. In Figure 56, all three gamma-ray peaks (662 keV from ^{137}Cs, 1.17 MeV and 1.33 MeV from ^{60}Co) can easily be observed when the directional detection system is aligned to 0°. Rotation of the system from 0° to 360° produces gamma-ray counts in each of the three CLYC detectors as presented in Tables 10, 11 and 12. The maximum statistical error

achieved in this measurement for CLYC #1 was 0.02%, for CLYC #2 was 0.02% and for CLYC #3 was 0.01%. It was observed from this data that the maximum counts occur for each source when CLYC #1 is rotated 0°, CLYC #2 is rotated 120° and CLYC #3 is rotated 240°. All three of these angles correspond to each detector aligning with the 0° hatch mark on the directional detection system turntable. This indicates that both sources are located at 0°. Processing this data through the MLE algorithm provides identical results; the ^{137}Cs and ^{60}Co source are both located at 0° as presented in Table 13.

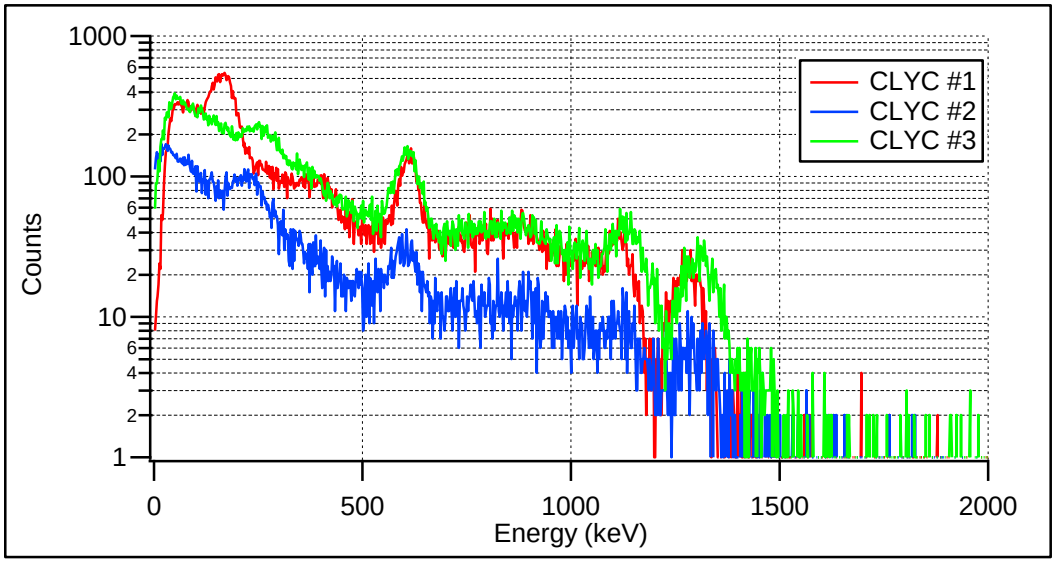

Figure 56 – Two source gamma-ray spectra at 0°, co-located sources

Table 10 – ^{137}Cs two source directional measurements results, co-located sources

Angle (degrees)	Counts in Photopeak		
	CLYC #1	CLYC #2	CLYC #3
0°	15252	4456	8396.017
40°	15171	7586	7185.212
80°	12339	10898.5	6196.185
120°	7933	16223.6	6323.806
160°	6297	13301.9	10103.14
200°	5105	8387.14	12635.43
240°	58312	6434.31	15251.81
280°	10061	3508.18	14535.57
320°	12706	5526.53	10339.87

Table 11 – ^{60}Co (1.17 MeV) two source directional measurements results, co-located sources

Angle (degrees)	Counts in Photopeak		
	CLYC #1	CLYC #2	CLYC #3
0°	4855.52	1467.46	2488.899
40°	4842.09	2201.43	2091.831
80°	3679.31	3315.96	1799.063
120°	2396.93	5302.99	2121.171
160°	1844.21	4780.69	2960.534
200°	1762.98	2825.32	4055.301
240°	1888.91	1857.91	4855.523
280°	3163.24	1101.92	4430.476
320°	4455.88	1779.4	3335.448

Table 12 – ^{60}Co (1.33 MeV) two source directional measurements results, co-located sources

Angle (degrees)	Counts in Photopeak		
	CLYC #1	CLYC #2	CLYC #3
0°	2902.1	861.286	1459.195
40°	2635.61	1215.59	1107.248
80°	1769.55	1683.25	1037.604
120°	1338.94	2591.11	1169.138
160°	1089.66	2256.58	1786.896
200°	739.702	1557.6	2217.39
240°	1228.37	1103.94	2902.097
280°	1900.05	624.63	2517.056
320°	2353.01	845.899	2076.116

Table 13 – Two source MLEA source direction estimates, co-located sources

Actual Source Position	Actual Source Direction	MLEA Source Direction	Error (%)
^{137}Cs: R=10 cm, z=0 cm	0°/360°	0°/360°	0
^{60}Co(1.17 MeV): R=10 cm, z=0 cm	0°/360°	0°/360°	0
^{60}Co (1.33 MeV): R=10 cm, z=0 cm	0°/360°	0°/360°	0

5.3.3 Neutron Measurements

In addition to the gamma-ray directional measurements, directional measurements were performed for the PuBe neutron source. The fast neutrons emitted from the PuBe source were thermalized using a polyethylene moderator. Measurements were collected

with the three-detector system in plane with the neutron beam from the PuBe source and at a longitudinal distance of 1 m and 3 m. The experimental setup is depicted in Figure 57 below. Measurements were collected at angles of 0°, 40°, 80°, 120°, 160°, 200°, 240°, 280° and 320°.

The results of the neutron directional measurements are displayed graphically in Figure 59 and 60. The maximum statistical error achieved in this measurement at R=1 m and at R=3 m was 0.02% for all CLYC detectors. The raw data populating these graphs accompanied by the MLE algorithm estimates for the neutron source direction are presented in Table 14. The source direction estimated by the MLE algorithm for the 1 m neutron measurements matched the physical direction of the neutron source. The estimated direction for the 3 m measurements was marginally off by 13.3°. This discrepancy in source direction can be eliminated by homogenizing the directional detection system as mentioned previously. It can also be eliminated by increasing the measurement time at each angle.

Table 14 – Thermal neutron source MLEA source direction estimates

Actual Source Position	**Actual Source Direction**	**MLEA Source Direction**	**Error (%)**
R=1 m, z=0 cm	0°/360°	0°/360°	0
R=3 m, z=-20 cm	0°/360°	13.33°	11.1

Figure 57 – Experimental setup for thermal neutron source directional measurements, R=1 m

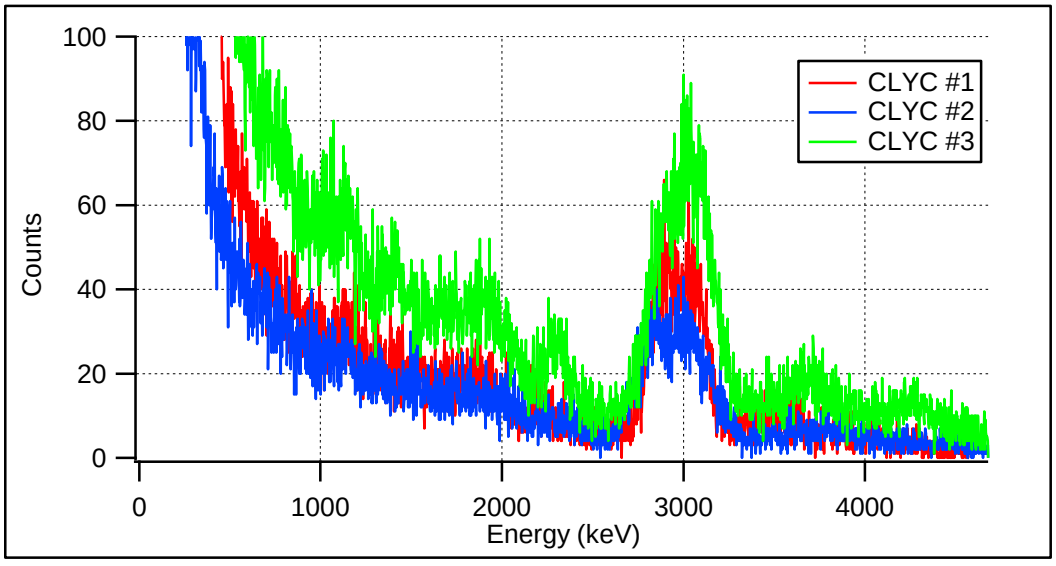

Figure 58 – Thermal neutron spectra at 0°

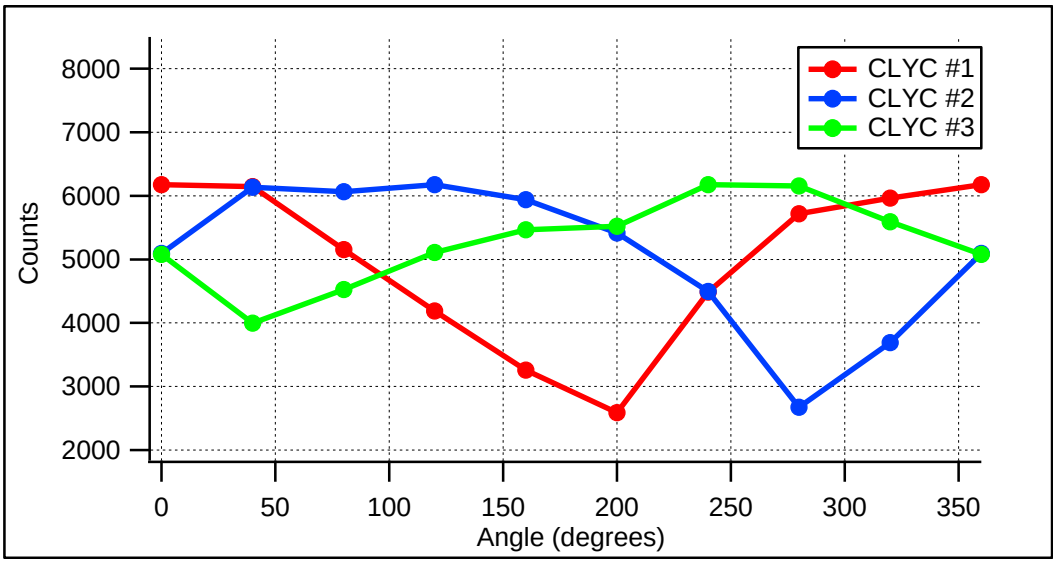

Figure 59 – Thermal neutron source directional measurements results, R=1 m, z=0 m

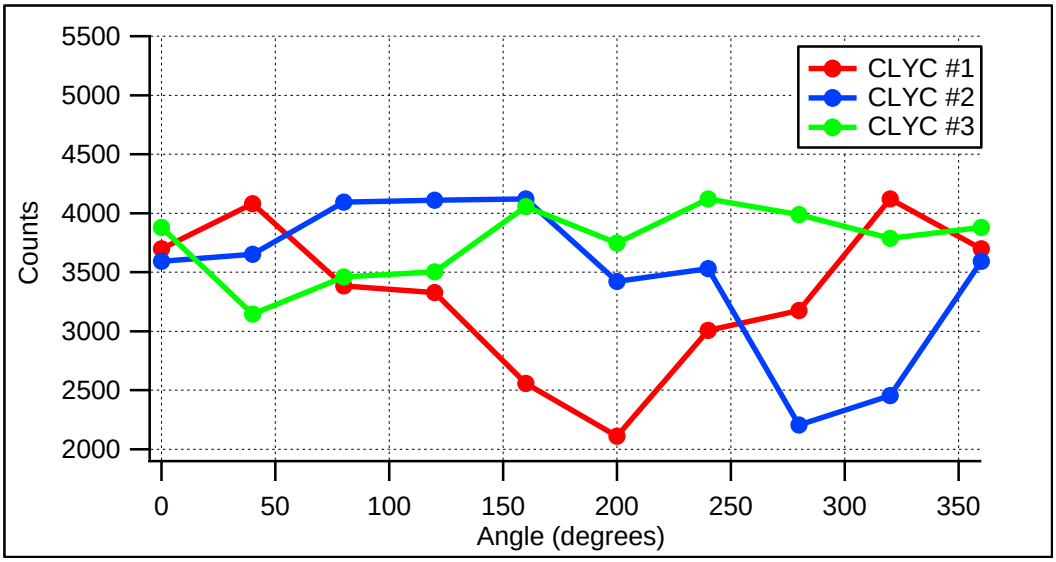

Figure 60 – Thermal neutron source directional measurements results, R=3 m, z=0 m

CHAPTER 6

CONCLUSIONS AND FUTURE WORK

The possibilities that lie within the atom are truly remarkable. As scientists and engineers continue to unravel these possibilities, unfortunately, the threat to homeland security grows. Neutron and photon detectors are essential to fulfilling mission areas of homeland security including detection and localization of missing, stolen or smuggled radiological or nuclear materials, quantification of the effects of a radiological or nuclear event, remote sensing and supporting nonproliferation efforts. Other areas benefitting by the advancement of radiation detection technology include treaty verification, power plant monitoring and nuclear medicine amongst many others. The elpasolite CLYC deployed as a dual neutron / gamma-ray directional detector provides means to improve the application of radiation detection in the aforementioned fields. This study explored the capabilities of CLYC as part of a directional detection system.

The computational element of this study evaluated the response of a CLYC scintillator to thermal neutron induced gamma rays created by a thermal neutron interaction with Cl and ^{7}Li nuclei. Arrays of three and four CLYC detectors were also modeled. The directional detection responses of each of these arrays were examined with both a thermal neutron source and a gamma-ray source. The responses of the three CLYC detector array provided means for comparison to the experimental directional detection study results. From this, it was demonstrated that the responses of the experimental study and the computational study agree well. The four-CLYC detector array served as a comparison to the three-CLYC detector array demonstrating that little or no quality would be lost when three detectors were used in the array. A three-detector system will

save cost, weight and reduce the dimensions of the system. In addition to the two previously mentioned computational models, a maximum likelihood estimation algorithm was developed to analyze the experimental and computational directional detection results providing an estimate for the unknown direction of a radioactive source.

The experimental study evaluated the photon spectroscopy capabilities of the 1-inch CLYC detector exposed to both ^{137}Cs and ^{60}Co. A gamma-ray energy resolution of 4.9% was achieved for the 662 keV peak of ^{137}Cs and 3.6% for the 1.33 MeV peak of ^{60}Co. When the CLYC detector was exposed to a thermal neutron source, pulse shape discrimination analysis was successfully performed. Thermal neutrons and gamma rays were separated with an outstanding FOM of 2.3. An array of three CLYC detectors was assembled for the purposes of directional neutron / gamma-ray detection. The intrinsic peak efficiency of three CLYC detectors was evaluated. The three-CLYC detector array was employed for directional measurements with a single gamma-ray source (^{137}Cs), two gamma-ray sources (^{137}Cs and ^{60}Co) and a thermal neutron source (PuBe with polyethylene moderator). Measurements were collected in the longitude and latitude planes over angles from 0° to 360°. The collected results were then processed through the maximum likelihood estimation algorithm providing an estimation of the direction for which the radioactive source in each case was positioned. The estimated directions provided were close if not an exact match for the actual direction of the radioactive source. The largest discrepancy in direction produced by the algorithm was about 11%. Compared to existing directional detection systems, this percent error is small. However, it was hypothesized that this error can be decreased by homogenizing the directional detection system to consist of scintillators of the same size and quality, identical

photomultiplier tubes and identical aluminum housings. The feasibility of this hypothesis to decrease the error was confirmed by the zero percent error achieved in the directional measurements produced in the computational study utilizing a homogenous directional detection system.

The computational and experimental studies described within this paper successfully evaluated the CLYC scintillator as a dual neutron / gamma-ray directional detector. Although much information about CLYC was gained in this study, much more progress is left to be made. Future endeavors with the CLYC detector include continued directional detection studies and directional detection system advancements. Assembling the three-CLYC detector array and the data acquisition system into one compact and wireless system with user-friendly interface capable of being deployed in the field is a next step. Continued directional measurements with different sources at different distances and heights in an "in-the-field" environment would be the next set of measurements to achieve. Another objective of future work is applying the directional detection system to remote sensing applications including unmanned aerial vehicle (UAV) and unmanned ground vehicle (UGV) based measurements. Source-search scenarios and radiation mapping can be achieved with these remote sensing techniques utilizing the directional detection system. In addition to continued directional detection system advancements, studying the CLYC as a fast neutron detector is a certain possibility. Utilizing the reaction of neutron interaction with ^{35}Cl in the CLYC producing a proton and ^{35}S, fast neutrons can be detected. The ideas and methods developed in this research will serve as a platform for these future endeavors and others working towards the deployment of CLYC as a dual neutron / gamma-ray directional detector.

APPENDICES

A.1 MCNP6 Input Code

A.1.1 Thermal Neutron Induced Gamma Rays Model

```
clyc1   Responce to Neutron Source
c  Gamma-ray and neutron fluences (spectral distr) in the CLYC scintillator
c   at the distance 20cm from the source.
c  Neutron source, isotropic: Thermal neutrons
c  Surrounding environment: void.
c cells begin
c detector cell
  10001  1   -3.31  -3        imp:n,p=1     $ CLYC
c Air in the world
  10041  4 -0.001205   -1 2 3  imp:n,p=1     $ air
c Source cage cell (air)
  10042  4 -0.001205   -2      imp:n,p=1     $ air
c outside world (void)
  10043  0         1  imp:n,p=0             $ outside, n,p-histories killed
c cells end

c surfaces begin
   1   rpp   -5. 35.  -10. 10.  -10. 10.     $ the world
   2   s     0.  0.  0.   0.1                $ small sphere to house the source
   3   rcc   20. 0.  0   7.62 0. 0.    3.81   $ detector
c surfaces end

mode  n p   $ neutrons and secondary gammas are transported
c  CLYC (Cs-2 Li Y Cl-6)
m1  55133 2.0 3006 1.0 39089 1.0 17000 6.0     $ (density = 3.31 g/cc)
c  Chlorine (nat abundance)
m2    17000 1.0          $ Cl-35 and Cl-37 (density = 2.17  g/cc)
c Salt (Na Cl)
m3  11022 1.0 17000 1.0   $ NaCl (density =  0.003214 g/cc)
c   Air, dry, near sea level
m4    6000.     -0.000124  7014.   -0.755268 &
      8016.     -0.231781 18000.   -0.012827 $ Air (density = 0.001205 g/cc)
sdef  erg=0.025e-6 pos=0. 0. 0.  cel=10042
c  Gamma-ray fluence (spectral distr) in the detector cell
f4:p 10001
e4   0.01 200i  11.0   $ 200 channels cover 0.01 - 11.0 MeV
c  Neutron fluence (spectral distr) in the detector cell
f14:n 10001
e14  0 200i  0.01e-5   $ 200 channels cover 0 - 0.01e-5
print
```

```
phys:n j 20 2j    $ physics for neutrons
phys:p  2j 0      $ physics for photons
ctme     30
```

A.1.2 Three Detector Directional Measurements Model with Thermal Neutron Source

```
1 0 -111 112 imp:n=1                                    $Detector Housing
2 1 -3.31 -112 imp:n=1                                  $CLYC
3 like 1 but trcl=(0 2.75 4.75)
4 like 1 but trcl=(0 -2.75 4.75)
5 like 2 but trcl=(0 2.75 4.75)
6 like 2 but trcl=(0 -2.75 4.75)
7 2 -0.001204 -113 111 #3 #4 #5 #6 imp:n=1
8 0 113 imp:n=0

111 rcc 0 0 -3  15 0 0 2.58                             $Detector Housing
112 rcc 0 0 -3  5.08 0 0 2.54                           $CLYC
113 sph 0 0 0 10000                                     $Air

m1  55133 2.0 3006 0.0759 3007 0.9241 39089 1.0 17000 6.0          $CLYC
m2  7014.70c  0.790    8016.70c  0.210     gas=1                   $Air
mode p
sdef par=p erg= 2.53e-8 pos=0 10 0
F8:n 2 5 6 T
FT8 CAP 3006
nps 1000000
print
```

A.1.3 Three Detector Directional Measurements Model with Gamma-ray Source

```
CLYC Detector Array - Three Detectors
1 0 -111 112 imp:n=1                                    $Detector Housing
2 1 -3.31 -112 imp:n=1                                  $CLYC
3 like 1 but trcl=(0 2.75 4.75)
4 like 1 but trcl=(0 -2.75 4.75)
5 like 2 but trcl=(0 2.75 4.75)
6 like 2 but trcl=(0 -2.75 4.75)
7 2 -0.001204 -113 111 #3 #4 #5 #6 imp:n=1
8 0 113 imp:n=0

111 rcc 0 0 -3  15 0 0 2.58                             $Detector Housing
112 rcc 0 0 -3  5.08 0 0 2.54                           $CLYC
113 sph 0 0 0 10000                                     $Air

m1  55133 2.0 3006 0.0759 3007 0.9241 39089 1.0 17000 6.0          $CLYC
```

```
m2  7014.70c  0.790    8016.70c  0.210     gas=1                    $Air
mode p
sdef par=p erg=0.662 pos=0 10 0
F4:p 2 5 6
nps 1000000
print
```

A.1.4 Four Detector Directional Measurements Model with Thermal Neutron Source

```
CLYC Detector Array - Four Detectors
1 0 -111 112 imp:n=1                                $Detector Housing
2 1 -3.31 -112 imp:n=1                              $CLYC
3 like 1 but trcl=(0 6 0)
4 like 1 but trcl=(0 0 6)
5 like 1 but trcl=(0 6 6)
6 like 2 but trcl=(0 6 0)
7 like 2 but trcl=(0 0 6)
8 like 2 but trcl=(0 6 6)
9 2 -0.001204 -113 111 #3 #4 #5 #6 #7 #8 imp:n=1
10 0 113 imp:n=0

111 rcc 0 -3 -3  15 0 0 2.58                        $Detector Housing
112 rcc 0 -3 -3  5.08 0 0 2.54                      $CLYC
113 sph 0 0 0 10000                                 $Air

m1  55133 2.0 3006 0.0759 3007 0.9241 39089 1.0 17000 6.0    $CLYC
m2  7014.70c  0.790    8016.70c  0.210     gas=1              $Air
mode p
sdef par=p erg= 2.53e-8 pos=0 10 0
F8:n 2 6 7 8
FT8 CAP 3006
nps 1000000
print
```

A.1.5 Four Detector Directional Measurements Model with Gamma-ray Source

```
CLYC Detector Array - Four Detectors
1 0 -111 112 imp:n=1                                $Detector Housing
2 1 -3.31 -112 imp:n=1                              $CLYC
3 like 1 but trcl=(0 6 0)
4 like 1 but trcl=(0 0 6)
5 like 1 but trcl=(0 6 6)
6 like 2 but trcl=(0 6 0)
7 like 2 but trcl=(0 0 6)
8 like 2 but trcl=(0 6 6)
```

```
9 2 -0.001204 -113 111 #3 #4 #5 #6 #7 #8 imp:n=1
10 0 113 imp:n=0

111 rcc 0 -3 -3  15 0 0 2.58                    $Detector Housing
112 rcc 0 -3 -3  5.08 0 0 2.54                  $CLYC
113 sph 0 0 0 10000                             $Air

m1  55133 2.0 3006 0.0759 3007 0.9241 39089 1.0 17000 6.0       $CLYC
m2  7014.70c  0.790    8016.70c  0.210     gas=1                 $Air
mode p
sdef par=p erg=0.662 pos=0 10 0
F4:p 2 6 7 8
nps 1000000
print
```

A.2 MATLAB Codes

A.2.1 Example of MATLAB Code for MLE Algorithm

```
clc,clear,close all
CLYC1=[2902.1 2635.61 1769.55 1338.94 1089.66 739.702 1228.37 1900.05 2353.01];
%CLYC #1 Counts
CLYC2=[861.286 1215.59 1683.25 2591.11 2256.58 1557.6 1103.94 624.63 845.899];
%CLYC #2 Counts
CLYC3=[1459.195004 1107.247989 1037.603958 1169.138302 1786.896328
2217.390419 2902.096634 2517.055816 2076.116389];    %CLYC #3 Counts
theta1=[0 40 80 120 160 200 240 280 320];   %CLYC #1 Angles
theta2=[120 160 200 240 280 320 360 400 440];   %CLYC #2 Angles
theta3=[240 280 320 360 400 440 480 520 560];   %CLYC #3 Angles
r=10;   %Distance from source to center of directional detection system
I0=28000;   %Estimate for source strength (number of gamma rays)
x1=[r*cosd(theta1)];    %x-coordinate of theta1
y1=[r*sind(theta1)];    %y-coordinate of theta1
x2=[r*cosd(theta2)];    %x-coordinate of theta2
y2=[r*sind(theta2)];    %y-coordinate of theta2
x3=[r*cosd(theta3)];    %x-coordinate of theta3
y3=[r*sind(theta3)];    %y-coordinate of theta3
C=mle(CLYC1)    %Calculates mean value of counts and uncertainty (enter either
CLYC1, CLYC2 or CLYC3)
sig1=C(2);      %Uncertainty (sigma) of counts
m=length(CLYC1);    %Calculates number of values in array
for i=1:m   %For loop calculates part 2 of log-likelihood function
   f(i)=(CLYC1(i)-(I0/(x1(i)^2-y1(i)^2)))^2;
end
F=m*log(1/(sqrt(2*pi)))-m*log(sig1)-(1/(2*sig1^2))*f;   %Log-likelihood function
G=-F;   %Multiply by negative to get max values of log-likelihood function
```

```
bar(theta1,G);  %Plot of log-likelihood function vs angle; direction of source at angle
with max log-likelihood value
```

REFERENCES

[1] D. A. Shea and D. Morgan, "The Helium-3 Shortage: Supply, Demand, and Options for Congress," *Federation of American Scientists*, 2010.

[2] J. R. Lamarsh and A. J. Baratta, Introduction to Nuclear Engineering Third Edition, Upper Saddle River, NJ: Prentice-Hall, Inc., 2001, pp. 238-242, 253-254, 533.

[3] "Evaluated Nuclear Data File (ENDF)," International Atomic Energy Agency, 14 March 2014. [Online]. Available: https://www-nds.iaea.org/exfor/endf.htm. [Accessed 6 August 2014].

[4] C. S. Shapiro, "Radioecology After Chernobyl," [Online]. Available: http://www.scopenvironment.org/downloadpubs/scope50/chapter01.html. [Accessed 6 August 2014].

[5] G. Knoll, Radiation Detection and Measurement Fourth Edition, United States: John Wiley & Sons, 2010.

[6] A. Guckes, A. Barzilov, D. Beller and T. Ward, "Monte Carlo Analysis of Neutron Multiplicity Detector System for WIMP Mass Measurement," in *Proc. American Nuclear Society Student Conference*, State College, PA, 2014.

[7] D. Shea and D. Morgan, "The Helium-3 Shortage: Supply, Demand, and Options for Congress," Congressional Research Service, 2010.

[8] Manticorp, "Scintillation Counter Schematic," 6 December 2011. [Online]. Available: http://tools.wmflabs.org/magnustools/flommons.pl?user=&mode=single_image& image=Scintillation_Counter_Schematic.jpg. [Accessed 5 August 2014].

[9] D. Reilly, N. Ensslin, H. S. Jr. and S. Kreiner, "Passive Nondestructive Assay of Nuclear Materials," 1991.

[10] P. A. Russo and D. T. Vo, "Gamma-ray Detectors for Nondestructive Analysis LA-UR-05-3813," Los Alamos National Laboratory, Los Alamos, NM.

[11] "Saint Gobain Data Sheet," Saint Gobain, 2014. [Online]. Available: http://www.crystals.saint-gobain.com/Plastic_Scintillators.aspx. [Accessed 4 August 2014].

[12] "Eljen Technology Data Sheet," Eljen Technology, [Online]. Available: http://www.eljentechnology.com/index.php/products/plastic-scintillators. [Accessed 4 August 2014].

[13] P. Guss and S. Mukhopadhyay, "Dual Gamma/Neutron Directional Elpasolite Detector," in *SPIE Conference on Penetrating Radiation Systems and Applications XIV*, San Diego, CA, 2013.

[14] J. Glodo, E. V. D. v. Loef, W. M. Higgins and S. Shah, "Cs2LiYCl6:Ce scintillator for nuclear monitoring applications," *IEEE Transactions on Nuclear Science,* 2009.

[15] J. Lejay, S. Blahuta, V. Ouspenski, P. Menge and D. Richaud, *Large CLYC:Ce and*

CLLB:Ce Crystals for Gamma-Neutron Detection Systems, Saint Gobain Crystals.

[16] C. M. Combes, P. Dorenbos, C. W. E. v. Eijk, K. Kramer and H. U. Gudel, "Optical and scintillation properties fro pure and Ce3+-doped Cs2LiYCl6 and Li3YCl6:Ce3+ crystals," *J. Lumin,* pp. 299-305, 1999.

[17] A. Bessiere, P. Dorenbos, C. W. E. v. Eijk, K. W. Kramer and H. U. Gudel, "New Thermal Neutron Scintillators: Cs2LiYCl6:Ce3+ and Cs2LiYBr6:Ce3+," *IEEE Transactions on Nuclear Science,* 2004.

[18] J. Glodo, W. M. Higgins, E. V. D. v. Loef and K. S. Shah, "Scintillation Properties of 1 Inch Cs2LiYCl6:Ce Crystals," *IEEE Transactions on Nuclear Science,* 2008.

[19] S. Mukhopadhyay, J. Glodo, R. Hawrami, E. V. D. v. Loef, W. M. Higgins, A. V. Churilov and K. shah, "Detection of Nuclear Material with Dual Neutron-Gamma Detector," *IEEE,* 2010.

[20] J. Glodo, E. V. D. v. Loef, R. Hawrami, W. M. Higgins, A. V. Churilov, U. Shirwadkar and K. S. Shah, "Selected Properties of Cs2LiYCl6, Cs2LiLaCl6, and Cs2LiLaBr6 Scintillators," *IEEE Transaction on Nuclear Science,* 2011.

[21] J. Glodo, E. V. D. v. Loef, R. Hawrami, U. Shirwadkar and K. S. Shah, "Pulse Shape Discrimination with Selected Elpasolite Crystals," *IEEE Transactions on Nuclear Science,* 2012.

[22] P. Guss, T. Stampahar, S. Mukhopadhyay, J. Lee, K. Shah, M. Squillante and W. Higgins, "Novel Deployment of Elpasolites as a Dual Gamma-Neutrons Directional

Detector," Site Directed Reseach & Development, Remote Sensing Laboratory-Nellis, 2013.

[23] P. Guss, "Novel Deployment of Elpasolites as a Dual Gamma Neutron Directional Detector," Site Directed Research & Development, Remote Sensing Laboratory-Nellis, 2014.

[24] D. Cooper, R. Ledoux, K. Kamieniecki, S. Korbly, J. Thompson, M. Ryan, N. Roza, L. Perry, D. Hwang, J. Costales and M. Kuznetsova, "Intelligent Radiation Sensor System (IRSS) Advanced Technology Demonstration (ATD)," *2010 IEEE International Conference on Technologies for Homeland Security (HST),* 2010.

[25] B. Deb, J. Ross, A. Ivan and M. Hartman, "Radioactive Source Estimation Using a System of Directional and Non-Directional Detectors," *IEEE Transactions on Nuclear Science,* vol. 58, no. 6, pp. 3281 - 3290 , 2011.

[26] E. Bogolubov, A. Koshelev, V. Mikerov and A. Sviridov, "Specific features of 3-D detection arrays of plastic scintillators," *Nuclear Instruments and Methods in Physics Research Section A: Accelerators, Spectrometers, Detectors and Associated Equipment,* vol. 652, no. 1, pp. 99-102, 2010.

[27] Y. Shirakawa, "Developments of directional detectors with NaI(Tl)/BGO scintillators," *Nuclear Instruments and Methods in Physics Research Section B: Beam Interactions with Materials and Atoms,* vol. 213, p. 255–259, 2004.

[28] RMD, Inc., "CLYC Properties," [Online]. Available: http://rmdinc.com/wp-

content/uploads/2013/03/CLYC_Properties.pdf. [Accessed 27 August 2014].

[29] Hamamatsu Photonics K. K., Hamamatsu, [Online]. Available: http://www.hamamatsu.com/us/en/product/category/3100/3001/R6231-100/index.html. [Accessed 28 August 2014].

[30] Hamamatsu Photonis K. K., Hamamatsu, [Online]. Available: https://www.hamamatsu.com/us/en/technology/innovation/photocathode/index.html. [Accessed 28 August 2014].

[31] Hamamatsu Photonics K. K., Hamamatsu, [Online]. Available: http://www.hamamatsu.com/us/en/product/category/3100/3001/R3998-100-02/index.html. [Accessed 28 August 2014].

[32] Bridgeport Instruments, LLC, "eMorpho MCA for Scintillator Detectors," July 2013. [Online]. Available: http://bridgeportinstruments.com/products/emorpho/emorpho_brief_u11.pdf. [Accessed 29 August 2014].

[33] Bridgeport Instruments, LLC, "eMorpho User Manual," June 2013. [Online]. Available: http://bridgeportinstruments.com/products/mds/mds_reference_v0m.pdf. [Accessed 30 August 2014].

[34] Bridgeport Instruments, LLC, "qMorpho 4-input DAQ for Scintillators," May 2012. [Online]. Available: http:bridgeportinstruments.com/products/qmorpho/qmorpho_brief_u5.pdf.

[Accessed 29 August 2014].

[35] Bridgeport Instruments, LLC, "hvBase - Plug-on High Voltage," Bridgeport Instruments, LLC, June 2010. [Online]. Available: http://bridgeportinstruments.com/products/hv_base/hvbase_brief_u4.pdf. [Accessed 3 September 2014].

[36] Wavemetrics, "IGOR Pro Overview," Wavemetrics, [Online]. Available: http://www.wavemetrics.com/products/igorpro/igorpro.htm. [Accessed 29 August 2014].

[37] M. Lone, R. Levitt and D. A. Harrison, "Prompt Gamma Rays from Thermal Neutron Capture," pp. 531-532, 1981.

[38] MCNP6 Development Team, *"MCNP6, Version1.0," Report LA-CP-13-00634,* Los Alamos National Laboratory, 2013.

[39] I. Akkurt, K. Gunoglu and S. S. Arda, "Detection Efficiency of NaI(Tl) Detector in 511 - 1332 keV Energy Range," *Science and Technology of Nuclear Installations,* 2014.

[40] M. Bourne, C. Mussi, E. Miller, S. Clarke, S. Pozzi and A. Gueorguiev, "Characterization of the CLYC detector for neutron and photon detection," *Nuclear Instruments and Methods in Physics Research Section A: Accelerators, Spectrometers, Detectors and Associated Equipment,* vol. 736, pp. 124-127, 2014.

VITA

Graduate College

University of Nevada, Las Vegas

Amber Guckes

Degree:

Bachelor of Science, Mechanical Engineering, 2013

University of Nevada, Las Vegas

Thesis Title: Novel Deployment of Elpasolites as a Dual Neutron / Gamma-Ray Directional Detector

Thesis Examination Committee:

Chairperson, Alexander Barzilov, Ph. D.

Committee Member, William Culbreth, Ph. D.

Committee Member, Denis Beller, Ph. D.

Graduate Faculty Representative, Ke-Xun Sun, Ph. D.